

WHAT ARE NARROW-LINE SEYFERT 1 GALAXIES?: TOWARD A VIEWING-ANGLE-DEPENDENT UNIFIED MODEL FOR SEYFERT GALAXIES

YOSHIAKI TANIGUCHI, TAKASHI MURAYAMA, & TOHRU NAGAO

Astronomical Institute, Graduate School of Science, Tohoku University, Aramaki, Aoba, Sendai 980-8578,
Japan

Submitted to the Astrophysical Journal

ABSTRACT

Narrow-line Seyfert 1 galaxies (NLS1s) have been recognized to comprise a distinct class of the Seyfert activity in addition to type 1 and type 2 Seyfert galaxies (S1s and S2s, respectively); the NLS1s show strong optical Fe II emission lines as well as high-ionization lines without optical broad emission lines. Recently growing evidence has been accumulated that the NLS1s are viewed from nearly pole-on viewing angles. However, there has been no theoretical model which explains the following important correlations; 1) weaker optical Fe II emitters always have wider emission-line widths but stronger optical Fe II emitters have either wider or narrower line widths, and 2) S1s with wider line widths always have flatter soft X-ray spectra but S1s with narrower line widths have either steeper or flatter soft X-ray spectra.

Photoionization models predict that the partly-ionized zone in the broad line region (BLR) with a disk-like configuration, in which the optical Fe II emission is thought to arise, is very optically thick; e.g., the hydrogen column density is required to be as high as $N_{\text{H}} \gtrsim 10^{24.5} \text{ cm}^{-2}$. Therefore, the visibility of the partly-ionized regions is expected to be strongly viewing-angle dependent. If we observe this disk-like BLR from an inclined viewing angle; e.g., $i_{\text{view}} \simeq 30^\circ$ [a typical viewing angle for broad-line S1s (hereafter BLS1s)], the Fe II emitting region located in the far-side half disk cannot be seen entirely because of the large optical depth while almost all the H β emission can be seen because the ionized hydrogen is located in the outer surfaces of BLR clouds. On the other hand, if we observe the disk-like BLR from a nearly pole-on view, we can see both Fe II and H β , resulting in a higher Fe II/H β ratio together with a narrower line width with respect to those observed from an inclined viewing angle. This explains the first important correlation.

Recent discovery of relativistic outflows in some NLS1s suggests that the nuclear radio jet interacts with the dense ambient gas very close to the central engine. We show that this can be responsible for the formation of hot plasma with kinetic temperatures of $T_{\text{kin}} \sim 10^6 \text{ K}$, giving rise to the production of soft X-ray photons. The black-body radiation from the hot plasma explains the observed steeper photon indices in the soft X ray if $T_{\text{kin}} \simeq (1 - 2) \times 10^6 \text{ K}$ and $\beta = v_{\text{jet}}/c \simeq 0.2 - 0.7$. The kinetic Doppler effect increases the soft X-ray luminosities if we observe S1s from a nearly pole-on view given the above range of β . These explain why NLS1s tend to have steeper soft X-ray spectra together with higher soft X-ray luminosities. Since the pole-on view model for NLS1s implies that BLS1s are viewed from intermediate orientations, the brightening due to the kinematic Doppler effect is generally weak for the BLS1s and thus the soft X-ray excess emission in the BLS1s is less dominant than that in the NLS1s. Furthermore, the extinction of soft X-ray photons due to dust grain above the dusty tori are expected to be more serious for the BLS1s than for the NLS1s. We thus suggest that these orientation effects are responsible for the second important correlation. It is also understood why soft X-ray surveys tend to pick up NLS1s preferentially.

It is known that there is a correlation between the soft X-ray photon index (Γ) and the Fe II $\lambda 4570/\text{H}\beta$ ratio for both NLS1 and BLS1s. We also newly find another correlation between Γ and the soft X-ray luminosity for the NLS1s studied by Boller, Brandt, & Fink. These correlations suggest that the strength of Fe II emission is intimately related to the soft X-ray emission. Since the ultraviolet continuum emission from the optically-thick accretion disk with $T \sim 10^5 \text{ K}$ cannot create partly-ionized regions in the disk-like BLR efficiently, we suggest that soft X-ray photons from the jet-driven shocked regions with $T \sim 10^6 \text{ K}$ are responsible for the formation of the Fe II emitting regions. This provides a causal relationship between the strong Fe II emission and the excess soft X-ray emission.

Finally, we propose a viewing-angle-dependent unified model for Seyfert nuclei; 1) $0^\circ \leq i_{\text{view}} \lesssim 10^\circ$ for NLS1s, 2) $10^\circ \lesssim i_{\text{view}} \lesssim 30^\circ$ for BLS1s, 3) $30^\circ \lesssim i_{\text{view}} \lesssim 50^\circ$ for type 2 Seyferts with the hidden BLR (S2⁺s), and 4) $50^\circ \lesssim i_{\text{view}} \leq 90^\circ$ for type 2 Seyferts without the hidden BLR (S2⁻s) where i_{view} is the viewing angle toward the BLR disk around the central engine. Since the NLS1 phenomenon is also observed in radio-quiet quasars, it is strongly suggested that the class of NLS1s is the radio-quiet equivalent of the class of Blazars in radio-loud active galactic nuclei.

Subject headings: galaxies: active - galaxies: Seyfert - quasars: general

arXiv:astro-ph/9910036v1 3 Oct 1999

1. INTRODUCTION

Seyfert nuclei are typical active galactic nuclei (AGN) in the nearby universe and their central engine is thought to be gas accretion onto a supermassive black hole (e.g., Rees 1984; Blandford 1990). The Seyfert nuclei have been broadly classified into two types based on the presence or absence of broad emission-line region (BLR) in their optical spectra (Khachikian & Weedman 1974); Seyferts with BLR are type 1 (hereafter S1) while those without BLR are type 2 (S2). These two types of Seyfert nuclei are now unified by introducing the viewing angle dependence toward the central engine given that a geometrically and optically-thick, dusty torus surrounds the central engine (Antonucci & Miller 1985; see for a review Antonucci 1993).

In addition to typical S1s and S2s, narrow-line Seyfert 1 galaxies (NLS1s) have also been recognized to comprise a distinct class of Seyfert nuclei since Davidson & Kinman (1978) noticed their particular observational properties [Koski 1978; Phillips 1978; Osterbrock & Pogge 1985 (hereafter OP85); Halpern & Oke 1987; van Groningen & de Bruyn 1989; Puchnarewicz et al. 1992, 1995a, 1995b; Mason, Puchnarewicz, & Jones 1996]. It is known that NLS1s share about ten percent of S1s in the hard X-ray selected sample (Stephens 1989). A large number of new NLS1s have been found in recent soft X-ray surveys of AGN [Puchnarewicz et al. 1992, 1996; Walter & Fink 1993; Boller, Brandt, & Fink 1996 (hereafter BBF96); Xu, Wei, & Hu 1999; Grupe et al. 1999; Edelson et al. 1999]. However, it is still not understood what the class of NLS1s is within the context of the current unified model. In order to construct a more perfect unified model of Seyfert nuclei, it is necessary to understand what NLS1s are and their relation to typical S1s and S2s.

In this paper, we give a summary of important observational properties of NLS1s (section 2) and possible models for NLS1s (section 3). Several observational tests are made in section 4. Kinematical and statistical considerations are given in sections 5 and 6, respectively. Then, in section 7, we propose a new model for NLS1s, which is consistent with almost all the observational properties of NLS1s. Finally, a viewing-angle-dependent unified model for Seyfert nuclei is presented in section 8. In order to avoid confusion, we refer typical S1s as broad-line Seyfert 1s (BLS1s). Therefore, it is meant that S1s = NLS1s + BLS1s.

2. OBSERVATIONAL PROPERTIES OF NLS1S

In this section, we give a summary of important observational properties of NLS1s in the optical, ultraviolet, soft and hard X rays, radio, and infrared. The individual items are labeled; e.g., [O1] (the first item in the optical), [O2] (the second item in the optical), and so on. We will refer the observational properties using these item codes in later discussion.

2.1. Optical

- [O1] Balmer emission lines are slightly broader than forbidden lines such as [O III] λ 5007 emission but their line widths (FWHMs) are typically $\simeq 1000 \text{ km s}^{-1}$ (Davidson & Kinman 1978; OP85; see also Mason, Puchnarewicz, & Jones 1996). The narrowest FWHM is $\approx 300 \text{ km s}^{-1}$ (Davidson & Kinman 1978;

OP85) while the widest one amounts to $\approx 2000 \text{ km s}^{-1}$ (Vaughan et al. 1999).

- [O2] The profiles of BLR emission of NLS1s are generally different from those of BLS1; i.e., a normal broad-line profile has a more dominant core than a NLS1 profile (Robinson 1995).
- [O3] The equivalent widths of Balmer emission lines are on average lower than those of BLS1s (OP85; Goodrich 1989); e.g., $\text{EW}(\text{H}\beta) \simeq 32 \pm 16 \text{ \AA}$ for the NLS1s and $\text{EW}(\text{H}\beta) \simeq 88 \pm 37 \text{ \AA}$ for the BLS1s (OP85).
- [O4] The time variability of Balmer emission lines is similar to that observed in BLS1s (Giannuzzo & Stripe 1996). However, there is a marginal trend that the variability in NLS1s is weaker than that in BLS1s (Giannuzzo et al. 1998).
- [O5] The [O III] λ 5007/H β ratio is smaller than 3 (OP85; Goodrich 1989).
- [O6] High-ionization emission lines like [Fe VII] λ 6087 and [Fe X] λ 6735 are present (Davidson & Kinman 1978; OP85; Nagao et al. 1999b). The [Fe VII] λ 6087/[O III] λ 5007 ratio of NLS1s is on average similar to that of BLS1s (Nagao, Murayama, & Taniguchi 1999a).
- [O7] Optical Fe II emission lines are generally stronger than those of BLS1s. There is a significant correlation between the Fe II λ 4570/H β intensity ratio and the FWHM of H β emission (Zheng & O'Brien 1990; Marziani et al. 1996); weak Fe II emitters always have larger FWHMs but stronger Fe II emitters have either larger or smaller FWHMs.
- [O8] Another correlation is found between Fe II λ 4570/H β and [O III] λ 5007/H β ; Fe II/H β tends to be stronger with decreasing [O III]/H β (Boroson & Green 1992).
- [O9] Spectropolarimetry of 17 NLS1s shows that no NLS1 has hidden BLR and the polarization detected in six NLS1s are attributed to the dust scattering rather than the electron scattering (Goodrich 1989); note that the polarization observed in most S2s is attributed to the electron scattering (Antonucci & Miller 1985; Miller & Goodrich 1990; Tran 1995).
- [O10] A summary of the emission-line components observed in NLS1s, BLS1s, and S2s is given in Table 1 (see also [U2]).

2.2. Ultraviolet

- [U1] Ultraviolet (UV) emission-line ratios (e.g., C IV λ 1549/Ly α) of NLS1s are similar to those of BLS1s (Crenshaw et al. 1991).
- [U2] Blue wing emission is present in UV emission lines, Ly α and C IV λ 1549. Their line widths amount to $\approx 5000 \text{ km s}^{-1}$, being comparable to those of BLS1s (Rodríguez-Pascual, Mas-Hesse, & Santos-Lleó 1997).
- [U3] The UV luminosities of NLS1s tend to be less luminous than those of BLS1s (Rodríguez-Pascual et al. 1997).

TABLE 1
UV/OPTICAL EMISSION-LINE COMPONENTS OBSERVED IN BLS1s, NLS1s, AND S2s

Component	HI-BLR ^a	LI-BLR ^b	NLR	HINER	Fe II
BLS1s	Yes	Yes	Yes	Yes	Yes
NLS1s	Yes	No	Yes	Yes	Yes
S2s	No	No	Yes	Yes/No	No

^aHigh-ionization BLR

^bLow-ionization BLR

2.3. X ray

- [X1] NLS1s tend to be stronger soft X-ray emitters with respect to BLS1s and often have ROSAT photon indices steeper than $\Gamma_{\text{soft}} = 3$ where the energy range is between 0.1 keV and 2.4 keV (Puchnarewicz et al. 1992; BBF96; Wang, Brinkmann, & Bergeron 1996; see for earlier indications Wilkes, Elvis, & McHardy 1987; Zheng & O'Brien 1990). The average photon index for the NLS1s is $\bar{\Gamma}_{\text{soft}} \simeq 3.13$ while that for the BLS1s is $\bar{\Gamma}_{\text{soft}} \simeq 2.34$ (BBF96)
- [X2] There is a significant correlation between the soft X-ray spectral index and the FWHM of $H\beta$ emission (Joly 1991; Zheng & O'Brien 1990); S1s with larger FWHM($H\beta$) (i.e., BLS1s) always have flat spectra but S1s with smaller FWHM($H\beta$) (i.e., NLS1s) emitters have either steep or flat spectra (BBF96; see also Lawrence et al. 1997).
- [X3] Hard X-ray spectra of NLS1s with steeper soft X-ray spectra are also steeper than those of BLS1s; 22 NLS1s studied with ASCA have 2 – 10 keV photon indices of $\Gamma_{\text{hard}} \simeq 1.6 - 2.5$ with a mean value of ~ 2.1 (Brandt, Mathur, & Elvis 1997; Leighly 1999b; Vaughan et al. 1999). Note that BLS1s have $\bar{\Gamma}_{\text{hard}} \approx 1.9$ (Nandra & Pounds 1994; Nandra et al. 1997).
- [X4] Broad absorption features centered in the energy range 1.1 – 1.4 keV or so-called warm absorption is found in $\approx 40\%$ (i.e., 9/22) of NLS1s (Leighly et al. 1997; Vaughan et al. 1999; Leighly 1999b). All these have narrower $H\beta$ line widths; FWHM $\lesssim 1000$ km s⁻¹ (Vaughan et al. 1999). However, it is noted that the detection rate of so-called warm absorbers in NLS1s appears lower than that in BLS1s (Wang et al. 1996; Leighly 1999b).
- [X5] Time variability in the soft X ray is often observed; the timescale is shorter than one day (BBF96). This corresponds to a size less than one light day, being smaller than the characteristic size of the BLR of BLS1s.
- [X6] Time variability is also observed in the hard X ray (Leighly 1999a). According to the time series analy-

sis based on the ASCA data of 24 NLS1s, the excess variance from the NLS1s light curves is inversely correlated with the X-ray luminosities. Furthermore, the excess variance for the NLS1s is flatter than that for BLS1s. The amplitude of the variability in the hard X ray is correlated with the strength of the soft excess; the NLS1s with stronger soft-excess tend to show the larger amplitude variability (Leighly 1999b).

- [X7] Soft X-ray observations show that there is no evidence for large neutral hydrogen column densities over the Galactic column, suggesting that the obscuration by dust grains is unimportant (BBF96).
- [X8] There is a positive correlation between Γ_{soft} and the UV (1375 Å)-to-X ray (2 keV) flux ratio for S1s and NLS1s follow this correlation (Walter & Fink 1993).

2.4. Radio

- [R1] The radio continuum luminosities of NLS1s lie in the range found for BLS1s (Ulvestad, Antonucci, & Goodrich 1995). However, as noted by them, their sample is not a statistically complete sample.
- [R2] The median radio size is no larger than 300 pc; i.e., most objects are not resolved by VLA observations (Ulvestad et al. 1995). Since the median radio size of BLS1s is 350 pc (Ulvestad & Wilson 1989), the NLS1s have radio sources with sizes similar to those in the BLS1s [here a Hubble constant $H_0 = 75$ km s⁻¹ Mpc⁻¹ is adopted].
- [R3] Among the seventeen NLS1s, only three have measurable radio axes; two NLS1s (Mrk 766 and Mrk 1126) have radio major axes perpendicular to the optical polarization while the remaining one (Mrk 957) has a radio major axis parallel to the optical polarization (Ulvestad et al. 1995).

2.5. Infrared

- [I1] Mid- and far-infrared luminosities based on IRAS observations (i.e., 12 μm , 25 μm , 60 μm , and 100 μm) of NLS1s are similar to those of BLS1s (Rodríguez-Pascual et al. 1997).

- [I2] The L -band ($3.5 \mu\text{m}$)-to-IRAS $25 \mu\text{m}$ flux ratio, which is sensitive to the orientation of dusty tori, of NLS1s is on average similar to that of BLS1s (Murayama et al. 1999; see also Murayama, Mouri, & Taniguchi 2000).

3. A SUMMARY OF PREVIOUS INTERPRETATIONS

Possible interpretations of NLS1s discussed previously are summarized below (see for good reviews BBF96; Giannuzzo & Stripe 1996). Note that five among the following seven models (I, II, III, V, and VI) assume that the BLR line width is dominated by the rotational motion around a central compact object.

- I) The pole-on view model (OP85; Goodrich 1989; Stephens 1989; Puchnarewicz et al. 1992): NLS1s are basically BLS1s but are viewed from a more face-on view (i.e., nearly pole-on view). This model requires that the BLR has a disk-like configuration.
- II) The low- M_{\bullet} model (Ross & Fabian 1993): NLS1s are basically BLS1s but their narrow line widths are attributed to the lower masses of the central black holes; e.g., $M_{\bullet} \sim 10^6 M_{\odot}$ for NLS1s while $M_{\bullet} \sim 10^7 M_{\odot}$ for BLS1s.
- III) The distant-BLR model (Mason et al. 1996): NLS1s are basically BLS1s but their narrow line widths are attributed to that the BLR in NLS1s is located at $r_{\text{BLR}} \sim 0.1 \text{ pc} - 1 \text{ pc}$. Note that a typical radial distance of the BLR in BLS1s is $\sim 0.01 \text{ pc}$ (e.g., Peterson 1993). A theoretical consideration for this model was given by Wandel & Boller (1998).
- IV) The no-BLR model (e.g., Giannuzzo & Stripe 1996): NLS1s are basically BLS1s but there is little gas in the BLR.
- V) The partly-hidden-BLR model (e.g., Giannuzzo & Stripe 1996): NLS1s are basically BLS1s but NLS1s are objects seen at relatively large inclination angles and thus only outer parts of the BLR can be seen. Since the outer parts of the BLR are seen in NLS1s, NLS1s are observed to be different from S2s whose BLR is completely hidden by dusty tori.
- VI) The intermediate-zone model (Mason et al. 1996): An intermediate-velocity ($\text{FWHM} \simeq 1000 \text{ km s}^{-1}$) line-emitting region produces significant amounts of the permitted and forbidden emission line fluxes in NLS1s. Since the estimated radial distance of this intermediate zone is $\sim 1 \text{ pc}$, this region is expected to be located between the BLR and the NLR (narrow-line region). The absence of the BLR in NLS1s is not understood solely by this model unless the intermediate zone is spatially identical to the distant BLR (see Model III).
- VII) A supermassive analog of Galactic black hole candidates (hereafter the GBHC model; Pounds et al. 1995): NLS1s are the supermassive black hole analogs of Galactic black hole candidates in the high state which are thought to be accreting at a larger fraction of the Eddington limit than those in the low state (e.g., Tanaka 1990).

4. OBSERVATIONAL TESTS

As summarized in section 3, there are seven possible models for the NLS1s. Since there are many interesting observational properties of the NLS1s as summarized in section 2, we can make various observational tests to reject some models.

4.1. Evidence Against the Distant-BLR Model

The distant-BLR model requires that the radial distance of the BLR is more distant than the typical value for BLS1s; i.e., $\sim 0.01 \text{ pc}$ (e.g., Peterson 1993). If we adopt a radial distance of the BLR of NLS1s $r_{\text{BLR}} = 0.1 \text{ pc}$, we obtain a maximum line width $\text{FWHM}^0(\text{BLR}) \approx 2 \times v_{\text{rot}} \simeq 1320 M_{\bullet,7}^{1/2} r_{\text{BLR},0.1}^{-1/2} \text{ km s}^{-1}$ where $v_{\text{rot}} = (GM_{\bullet}/r_{\text{BLR}})^{1/2}$ is the Keplerian rotational velocity and $M_{\bullet,7}$ is the mass of the supermassive black hole in units of $10^7 M_{\odot}$. Thus this model explains the narrow line widths of the BLR emission. However, Robinson (1995) found that the profiles of BLR emission of NLS1s are generally different from those of BLS1; i.e., a normal broad-line profile has a more dominant core than a NLS1 profile [O2]. This property cannot be explained by the distant-BLR model.

The optical monitoring observations of NLS1s promoted by Giannuzzo and coworkers have shown that there is no significant difference between the optical variability properties of NLS1s and BLS1s [O4]. This provides also evidence against the distant-BLR model.

Recently, Wandel & Boller (1998) proposed a theoretical basis for the distant-BLR model; a stronger photoionizing continuum present in NLS1s can be responsible for the ionization of BLR clouds at larger radii where the Keplerian velocities are lower. However, in their model, it is not well understood why only NLS1s have such stronger-photoionizing continua. Therefore, in order to accept this model, one will have to explain the origin of the stronger continuum emission. Furthermore, if we adopt this model, the number ratio between NLS1s and BLS1s can be attributed to a variety of the radial distance of BLR in Seyfert nuclei. There may be many parameters to determine r_{BLR} in each Seyfert; the dynamical stability of a rotating gaseous disk (or a ring) around a SMBH, the angular momentum of the BLR gas, the phase of gas accretion, and so on. Therefore, at present, this model may not give a self-consistent explanation of NLS1s.

4.2. Evidence Against the No-BLR Model

It has been considered that the intense soft X-ray emission can prevent the formation of the BLR clouds close to the central engine (Guilbault, Fabian, & McCray 1983; White, Fabian, & Mushotzky 1984). However, although there is no evidence for the BLR in the optical spectra of NLS1s, Rodríguez-Pascual et al. (1997) found the blue wing emission in UV emission lines, $\text{Ly}\alpha$ and $\text{C IV}\lambda 1549$ [U2]. Since the line widths of the blue wing emission amount to $\approx 5000 \text{ km s}^{-1}$, it turns out that the NLS1s observed by them have the BLR. Accordingly, we can reject the no-BLR model.

However, one problem remains. Why do only UV lines show evidence for the BLR while there is no evidence for the BLR in the optical? Since the UV BLR shows the

blue wing emission, it is likely that the UV BLR is associated with some outflow activity. This means that there are two kinds of BLR; one is the disk-like BLR which emits optical Blamer lines and the other is the jet-like BLR which emits UV BLR emission lines like Ly α and C IV (see section 7.2 for more detail). This picture appears consistent with the recent analysis of UV and optical emission lines of AGN (Sulentic et al. 1995; Marziani et al. 1996; see also Dultzin-Hacyan, Taniguchi, & Uranga 1999; Taniguchi, Dultzin-Hacyan, & Murayama 1999).

4.3. Evidence Against the Intermediate-Zone Model

Mason et al. (1996) found the intermediate-velocity (FWHM $\simeq 1000$ km s $^{-1}$) line-emitting region which produces significant amounts of the permitted and forbidden emission line fluxes in one of NLS1s, RE J1034+396. However, the estimated radial distance of this intermediate zone, ~ 1 pc, is similar to that of the inner wall of dusty tori (e.g., Taniguchi & Murayama 1998 and references therein). If the line width of the rotational motion of the dusty tori, we obtain FWHM $\simeq 1320M_{\bullet,8}^{1/2}r_1^{-1/2}$ km s $^{-1} \simeq 1320M_{\bullet,7}^{1/2}r_{0.1}^{-1/2}$ km s $^{-1}$ where $M_{\bullet,8}$ and $M_{\bullet,7}$ are the black hole mass in units of 10^8M_{\odot} and 10^7M_{\odot} , respectively, and r_1 and $r_{0.1}$ are the radial distance of the inner wall in units of 1 pc and 0.1 pc, respectively. Since the inner wall of dusty tori is one of the important emission-line regions (Pier & Voit 1995; Murayama & Taniguchi 1998a, 1998b; Kramer et al. 1998), the modest interpretation for the intermediate zone found by Mason et al. (1996) is that such intermediate-velocity (i.e., FWHM $\simeq 1000$ km s $^{-1}$) lines arise from the inner wall of dusty tori (cf. Sulentic & Marziani 1998). Therefore, the presence of such intermediate-velocity line-emitting regions may not be an essentially important property of the NLS1s.

4.4. Evidence Against the Partly-Hidden-BLR Model

The partly-hidden-BLR model means that NLS1s are objects seen at relatively large inclination angles and thus only the outer parts of the BLR can be seen; i.e., NLS1s could be regarded as an intermediate class between BLS1s and S2s. Since this model allows the presence of inner parts of the BLR, this is different from the distant-BLR model.

However, if this is the case, the optical spectropolarimetry could detect hidden BLRs in the polarized spectra of NLS1s. However, Goodrich (1989) could not find any evidence for the hidden BLR [O9]. Although he found the polarized continuum emission in six NLS1s among 18, the polarization is attributed to the scattering by dust grains rather than free electrons. Dust grains which produce the observed polarization may be located either in the NLR (e.g., Netzer & Laor 1993) or in the inner wall of dusty tori. Since the polarization of S2s is attributed to the electron scattering (Antonucci & Miller 1985; Miller & Goodrich 1990; Tran 1995), it is unlikely that NLS1s are viewed from nearly the same viewing angles as those for S2s.

It is known that the inner wall of dusty tori produces the high-ionization emission lines such as [Fe VII] and [Fe X] because this region has a larger ionization parameter and relatively higher electron densities, e.g., $n_e \sim 10^{7-8}$ cm $^{-3}$ (e.g., Pier & Voit 1995; Murayama & Taniguchi 1998b).

Murayama & Taniguchi (1998a) found that S1s have excess [Fe VII] $\lambda 6087$ emission with respect to S2s and proposed that the high-ionization nuclear emission-line region (HINER: Binette 1985; Murayama, Taniguchi, & Iwasawa 1998) traced by the [Fe VII] $\lambda 6087$ emission resides in the inner wall of dusty tori. Murayama & Taniguchi (1998b) constructed new dual-component (i.e., a typical NLR with a HINER torus) photoionization models and showed that the observations are well explained if the torus emission contributes to ~ 10 % of the NLR emission. Therefore, the significant excess emission of such high-ionization lines in BLS1s can be attributed to the relative importance of the torus HINER with respect to S2s. Recently, Nagao et al. (1999a) found that the strength of [Fe VII] $\lambda 6087$ emission relative to [O III] $\lambda 5007$ of NLS1s is similar on average to that of BLS1s. Therefore, the viewing angles to the dusty tori for NLS1s are not different significantly from those for BLS1s.

Recently Murayama et al. (1999) made a mid-infrared test for NLS1s. They compared the *L*-band (3.5 μ m)-to-IRAS 25 μ flux ratio, which is sensitive to the orientation of dusty tori, among NLS1s, BLS1s, and S2s and found that the ratio of NLS1s is on average similar to that of BLS1s. This suggests again that the average viewing angles toward the NLS1s are not different significantly from those toward the BLS1s.

All the above observations appear to be inconsistent with the partly-hidden-BLR model. Thus we can reject this model.

5. KINEMATICAL CONSIDERATION

5.1. Introduction

Among the seven models, we have rejected the four models; the distant-BLR model, the no-BLR model, the intermediate-zone model, and the partly-hidden-BLR model. We also do not consider the GBHC model in later discussion although we will give some comments on this model in section 7.4. Now the following two models remain; the pole-on view model, and the low- M_{\bullet} model. Prior to going to construct a possible model for NLS1s, we investigate these two models from kinematical points of view.

A typical FWHM of the BLR of BLS1s is 5000 – 10000 km s $^{-1}$ (e.g., Osterbrock 1989; Peterson 1997; Eracleous & Halpern 1994). Although double-peaked BLR profiles with FWHM ~ 12000 km s $^{-1}$ are also found in a large number of AGN, they are more often found in radio-loud AGN (Steiner 1981; Eracleous & Halpern 1994). Since our main purpose is to investigate the origin of NLS1s (i.e., radio-quiet AGN), we adopt FWHM(BLR) = 6000 km s $^{-1}$ for BLS1s in this discussion (Eracleous & Halpern 1994).

Recent reverberation mapping for a large number of BLS1s has shown that the line widths of the BLR are dominated by the rotational motion (e.g., Peterson 1993; Wanders et al. 1995). One important aspect is that there are two alternative options for the geometrical properties of the BLRs; a disk-like configuration or a jet-like one. Recently Rodríguez-Pascual et al. (1997) found the blue wing emission in UV emission lines, Ly α and C IV $\lambda 1549$ in some NLS1s [U2], implying the presence of the jet-like BLR. Even though, these NLS1s have narrower op-

tical BLR emission lines (i.e., H α , H β , and Fe II) whose FWHMs are $\approx 1000 \text{ km s}^{-1}$. It seems reasonable to assume that these narrower optical BLR lines arise from the disk-like BLR.

5.2. An Intrinsic FWHM of the Disk-like BLR

First let us estimate an intrinsic FWHM of the BLR in BLS1s. Although we adopt $\text{FWHM}(\text{BLR}) = 6000 \text{ km s}^{-1}$ for BLS1s, this is not an intrinsic one because we do not always observe the BLR disk from a perfect face-on view. In fact, the MIR test [I2] suggests that the viewing angle toward the dusty tori of BLS1s lies in a range between 0° and $30^\circ - 45^\circ$ (Murayama et al. 1999, 2000). Although either the BLR disk or the dusty torus or both may be warped more or less (Pringle 1997; Nishiura, Murayama, & Taniguchi 1998), it is likely that we observe the BLR disk in BLS1s from nearly the same viewing angles estimated above for the dusty tori. It is also reported that the inner accretion disk probed by Fe K line in the hard X ray is inclined by $\simeq 30^\circ$ to the lines of sight for a large number of BLS1s (e.g., Tanaka et al. 1995; Nandra et al. 1997). Therefore, it seems reasonable to assume that an average viewing angle to BLS1s is $\bar{i}_{\text{view}} \approx 30^\circ$. Then we obtain an intrinsic FWHM of the BLR in BLS1s,

$$\text{FWHM}^0(\text{BLR}) = \frac{\text{FWHM}(\text{BLR})}{\sin \bar{i}_{\text{view}}} = 12000 \text{ km s}^{-1}. \quad (1)$$

It is noted that this intrinsic FWHM is almost comparable to a typical FWHM of the double-peaked BLR (Eracleous & Halpern 1994).

We examine whether or not the simple Keplerian rotation is responsible for this line width. If we adopt $M_\bullet = 10^7 M_\odot$ and $r_{\text{BLR}} = 0.01 \text{ pc}$, we obtain $\text{FWHM}^0(\text{BLR}) = 2 v_{\text{rot}} \simeq 4200 M_{\bullet,7}^{1/2} r_{\text{BLR},0.01}^{-1/2} \text{ km s}^{-1}$ where $M_{\bullet,7}$ is the black hole mass in units of $10^7 M_\odot$ and $r_{\text{BLR},0.01}$ is the radial distance of the BLR from the galactic nucleus in units of 0.01 pc. The mass of supermassive black holes in BLS1s lies in a range between $10^7 M_\odot$ and $10^8 M_\odot$ (e.g., Miyoshi et al. 1995; Greenhill et al. 1996; Nishiura & Taniguchi 1998 and references therein). If we adopt $M_\bullet = 10^8 M_\odot$, we obtain

$$\text{FWHM}^0(\text{BLR}) \simeq 13200 M_{\bullet,8}^{1/2} r_{\text{BLR},0.01}^{-1/2} \text{ km s}^{-1}. \quad (2)$$

The following combinations also give the same $\text{FWHM}^0(\text{BLR})$; $(M_\bullet, r_{\text{BLR}}) = (10^7 M_\odot, 0.001 \text{ pc})$, and $(3 \times 10^7 M_\odot, 0.003 \text{ pc})$. Therefore, the intrinsic FWHM for the BLR appears to be explained by the disk rotation without invoking other motions.

5.3. Origin of the Narrow FWHM of NLS1s

Next we consider why $\text{FWHM}(\text{BLR}) \simeq 1000 \text{ km s}^{-1}$ for NLS1s for the following two cases: 1) the pole-on view model, and 2) the low- M_\bullet model.

1) The pole-on view model: This model implies that the observed narrow FWHMs for NLS1s are attributed to smaller viewing angles toward the BLR. Therefore, given the intrinsic FWHM of the BLR in S1s $\text{FWHM}^0(\text{BLR}) \simeq 12000 \text{ km s}^{-1}$ with the typical $\text{FWHM}(\text{BLR}) \simeq 1000 \text{ km}$

s^{-1} for the NLS1s, we obtain a critical viewing angle toward NLS1s $i_{\text{cr,NLS1}} \simeq \sin^{-1}(1000 \text{ km s}^{-1}/12000 \text{ km s}^{-1}) \simeq 4.8^\circ$; i.e., $0^\circ \leq i_{\text{view}} \leq i_{\text{cr,NLS1}}$ for NLS1s. On the other hand, if we adopt the maximum value of $\text{FWHM}(\text{BLR}) \simeq 2000 \text{ km s}^{-1}$ for NLS1s (Vaughan et al. 1999), we obtain $i_{\text{cr,NLS1}} \simeq 9.6^\circ$. This seems to be a more appropriate estimate.

2) The low- M_\bullet model: If we adopt $M_\bullet = 10^6 M_\odot$, we obtain $\text{FWHM}^0(\text{BLR}) \simeq 1320 M_{\bullet,6}^{1/2} r_{\text{BLR},0.01}^{-1/2} \text{ km s}^{-1}$. Since the optical reverberation mapping shows that the shortest variability timescale is about one week, i.e., corresponding to a linear dimension $\sim 0.01 \text{ pc}$ (e.g., Peterson 1993), the mass of SMBHs is required to be less massive than $10^6 M_\odot$. The dynamical mass of nuclei has been estimated for a number of BLS1s (Wandel & Yahil 1985; Padovani & Rafanelli 1988; Padovani, Burg, & Edelson 1989; Padovani 1989; Koratkar & Gaskell 1991) and for S2s with the hidden BLR (Nishiura & Taniguchi 1998). However, there is no dynamical estimate for the nuclei of NLS1s. Recently Hayashida et al. (1998; see also Hayashida 1997) proposed a new method to estimate the central black hole masses based on the X-ray flux variability. They obtained $M_\bullet \simeq 4.93 \times 10^4 M_\odot$ for one of NLS1s, NGC 4051. This mass is smaller by two or three orders of magnitude than the typical mass of Seyfert nuclei. Indeed, the recent reverberation mapping gives $M_\bullet \simeq 1.4 \times 10^6 M_\odot$ for NGC 4051 (Wandel, Peterson, & Malkan 1999). It is noted that their method tends to give a smaller mass than the dynamical method (e.g., Koratkar & Gaskell 1991). For example, Hayashida et al. (1998) obtained $M_\bullet \simeq 9.16 \times 10^6 M_\odot$, $1.90 \times 10^7 M_\odot$, and $1.79 \times 10^7 M_\odot$ for NGC 4151, NGC 5548, and 3C 273, respectively. On the other hand, Koratkar & Gaskell (1991) obtained $M_\bullet \simeq 3.2 \times 10^7 M_\odot$, $2.2 \times 10^8 M_\odot$, and $3.5 \times 10^8 M_\odot$ for the same galaxies. Although we do not know which method is more reliable, it will be necessary to estimate the black hole mass for both BLS1s and NLS1s with a consistent manner.

6. STATISTICAL CONSIDERATION

6.1. Frequency of Occurrence of NLS1s

Stephens (1989) show that NLS1s share $\approx 10\%$ of S1s based on optical spectroscopy of 65 hard X-ray selected AGN. The number of NLS1s has been increasing by means of soft X-ray surveys of AGN (Puchnarewicz et al. 1992, 1996; BBF96; Xu et al. 1999). Indeed, NLS1s comprise about half of the AGN in soft X-ray selected samples (Grupe et al. 1999; Edelson et al. 1999). However, since soft X-ray photons are easily absorbed by dense gas clouds in nuclear regions of Seyfert galaxies (e.g., Awaki et al. 1991), any soft X-ray selected samples tend to miss such obscured AGN, giving rise to the overabundance of both NLS1s and BLS1s. Hard X-ray, radio, or optical surveys are more useful for any statistical considerations. Therefore, we adopt the fraction obtained by Stephens (1989).

6.2. Interpretation Based on the Pole-on View Model

If we adopt the pole-on view model for NLS1s, the fraction of NLS1s gives a critical viewing angle to NLS1s statistically by the following relation,

$$\frac{N_{\text{NLS1}}}{N_{\text{S1}} + N_{\text{S2}}} = \frac{N_{\text{NLS1}}}{N_{\text{NLS1}} + N_{\text{BLS1}} + N_{\text{S2}}}$$

$$= 1 - \cos i_{\text{cr,NLS1}} \quad (3)$$

where N_{NLS1} , N_{BLS1} , and N_{S2} are the numbers of NLS1s, BLS1s, and S2s, respectively. According to Stephens (1989), we have

$$\frac{N_{\text{NLS1}}}{N_{\text{S1}}} = \frac{N_{\text{NLS1}}}{N_{\text{NLS1}} + N_{\text{BLS1}}} = 0.1. \quad (4)$$

The number ratio between S1s and S2s is obtained by the following surveys; 0.125 (Osterbrock & Shaw 1988), 0.20 (Salzer 1989), and 0.435 (Huchra & Burg 1992). Note that these ratios are corrected for the completeness of the individual surveys. The simple average of the three surveys gives 0.25 ± 0.13 . It is noted that this ratio gives a critical viewing angle to BLS1s is $i_{\text{cr,BLS1}} \simeq 37^\circ$. This value is almost consistent with the opening angle of NLRs; $26^\circ \pm 11^\circ$ (Pogge 1989), $32^\circ \pm 8^\circ$ (Wilson & Tsvetanov 1994), and $29^\circ \pm 9^\circ$ (Schmitt & Kinney 1996). Therefore, the above average ratio appears reasonable. Since NLS1s are included in the samples of S1s, we adopt

$$\frac{N_{\text{S1}}}{N_{\text{S2}}} = \frac{N_{\text{NLS1}} + N_{\text{BLS1}}}{N_{\text{S2}}} = 0.25. \quad (5)$$

Using equations (1), (2), and (3), we obtain $i_{\text{cr,NLS1}} \simeq 10.9^\circ$. Although this value is slightly larger than the previous estimate based on the kinematical considerations [4.8° for $\text{FWHM}(\text{BLR}) = 1000 \text{ km s}^{-1}$ and 9.6° for $\text{FWHM}(\text{BLR}) = 2000 \text{ km s}^{-1}$], there may be no serious inconsistency between the two estimates if the observational ambiguities in both the estimates are taken into account.

6.3. Interpretation Based on the Low- M_\bullet Model

If we adopt the low- M_\bullet model, the number ratio between NLS1s and BLS1s can be attributed to the mass function of SMBHs in Seyfert nuclei. Therefore, a direct way to prove this model is to show that NLS1s have systematically lower black hole masses than BLS1s. However, as mentioned in section 5.3, there is no reliable comparison of the black hole mass between NLS1s and BLS1s. Recent high-resolution optical spectroscopy observations have shown that SMBHs with $M_\bullet \sim 10^{6-9} M_\odot$ are present in nearby galaxies and there is a relationship between the SMBH mass and the spheroidal mass of galaxies; i.e., $M_\bullet \approx 0.006 M_{\text{sph}}$ (Kormendy et al. 1998). It will become important to compare the spheroidal mass between NLS1s' and BLS1s' host galaxies.

7. A NEW MODEL

7.1. Introduction

As described in section 4, it is hard to discriminate which model is more plausible among the two, the pole-on view model or the low- M_\bullet one. Here it is remembered that there are two important correlations (section 2); [O7] the correlation between Fe II/ $H\beta$ intensity ratio and the FWHM of $H\beta$ emission; weak Fe II emitters always have larger FWHMs but stronger Fe II emitters have either larger or smaller FWHMs, and [X2] the correlation between the soft X-ray spectral index and the FWHM of $H\beta$ emission; S1s with larger $\text{FWHM}(H\beta)$ (i.e., BLS1s) always have flat spectra but S1s with smaller $\text{FWHM}(H\beta)$ (i.e., NLS1s) emitters have either steep or flat spectra.

If we adopt the low- M_\bullet , a tunable parameter is only the black hole mass. It seems difficult to explain the above two correlations by tuning only M_\bullet . On the other hand, the pole-on view model has the viewing-angle dependence which is known to affect the visibility of some emission line components because of the effect of selective obscuration. Although it is natural that there is a scatter in M_\bullet from galaxy to galaxy, we try to find a possible model adopting the viewing angle as the primary parameter.

7.2. The Fe II Emitting Region

We begin our model with a question; ‘‘Where is the Fe II emitting region?’’ The reason for this is that the Fe II emission is unusually strong in NLS1s with respect to BLS1s [O7]. It has been often considered that the Fe II emission arises from partly ionized regions heated by X-ray photons (Ferland & Netzer 1979; Kwan & Krolik 1981). Since S2s show no Fe II features in the optical spectra, the current unified model for Seyfert nuclei suggests that the Fe II emitting regions should be inside the dusty tori. Therefore, the most natural place is considered to be optically-thick ionization-bounded clouds located in the BLR (Collin-Souffrin & Lasota 1988; Collin-Souffrin, Hameury, & Joly 1988; Marziani et al. 1996; Dultzin-Hacyan et al. 1999).

One of the important observational properties of NLS1s is the evidence for the blue wing emission in UV emission lines, $\text{Ly}\alpha$ and $\text{C IV}\lambda 1549$ [U2]. Since their line widths amount to $\approx 5000 \text{ km s}^{-1}$, there is a highly-ionized BLR (hereafter HI-BLR) even in NLS1s. It has been suggested that the HI-BLR is associated with the jet-like BLR (Marziani et al. 1996; Dultzin-Hacyan et al. 1999; see also Sulentic et al. 1995). Marziani et al. (1996) present the first direct comparison between the HI-BLR (e.g., C IV) and the low-ionization BLR (hereafter LI-BLR) (e.g., $H\beta$) for a sample of 52 radio-quiet AGN. They found the following correlations; the C IV equivalent width $\text{EW}(\text{C IV})$ decreases with (a) increasing blueshift of C IV relative to $H\beta$ (broad component), (b) increasing strength of the optical Fe II multiplets, and (c) increasing strength of the optical-UV continuum. These correlations and the systematic nature of the C IV blueshift relative to $H\beta$ suggest a model where: (i) C IV emitting clouds show a predominance of radial motion (outflow because it is assumed that the far side is obscured) in a bi-conical (and/or disk wind) structure with a wide opening angle; i.e., the jet-like BLR. (ii) Fe II optical emission arises in a flattened distribution (possibly an accretion disk); i.e., the disk-like BLR, and (iii) $H\beta$ arises in a different and less flattened distribution.

Taking these properties into account, we adopt the following simple two-component BLR model in the later discussion; 1) the disk-like BLR in which Fe II and $H\beta$ arise, and 2) the jet-like BLR in which C IV and $\text{Ly}\alpha$ arise (see Figure 1). Even in the disk BLR, the gas is distributed in a clumpy form because the volume filling factor in the BLR is generally low; e.g., $\sim 10^{-7}$ (Peterson 1997). If we assume that each BLR cloud has a spherical form, the outer surface facing to the central engine is highly ionized (e.g., Pier & Voit 1995). Therefore, it is considered that the Fe II emitting region is partly ionized zones which are shaded by highly- and intermediately-ionized zones from the central engine. A possible formation mechanism of partly-ionized regions in the disk-like BLR will be discussed in section

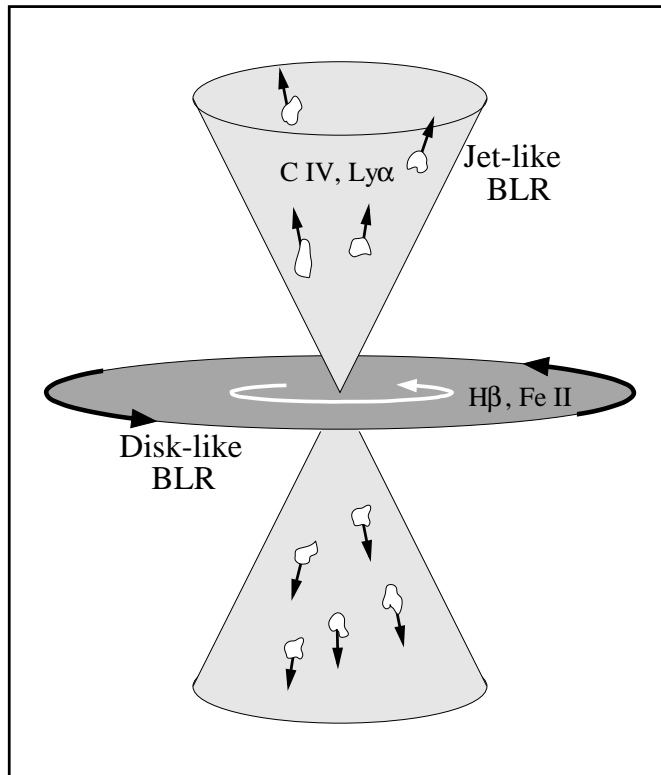


FIG. 1.— A schematic illustration of the two-component BLR model. This is reproduced from Figure 3 in Dultzin-Hacyan et al. (1999).

7.4.

There is no direct information about the optical depth from the central engine toward the Fe II emitting region. However, we can infer it using observations and theoretical considerations on infrared Ca II triplet lines at 8498 Å, 8542 Å, and 8662 Å (Persson 1988; Ferland & Persson 1989; Joly 1989) which are also considered to arise from the same partly-ionized regions as those of the Fe II emission (Dultzin-Hacyan et al. 1999; Taniguchi et al. 1999). Comparing photoionization models with the observations, Ferland & Persson (1989) found that optically thin clouds with column densities $N_{\text{H}} \sim 10^{23} \text{ cm}^{-2}$ cannot reproduce the observed Ca II triplet line ratios regardless of density and ionization parameters. The observed Ca II spectra can be reproduced if $N_{\text{H}} \gtrsim 10^{24.5} \text{ cm}^{-2}$. Therefore, the visibility of the partly-ionized regions is expected to be strongly viewing-angle dependent. If we observe this disk-like BLR from an inclined viewing angle (e.g., $i_{\text{view}} = 30^\circ$), the Fe II emitting region located in the far-side half disk cannot be seen entirely because of the large optical depth. On the other hand, the $\text{H}\beta$ emission can be seen from the entire BLR disk because the ionized hydrogen is located in the outer surfaces of BLR clouds. On the other hand, if we observe the disk-like BLR from a nearly pole-on view, we can see both Fe II and $\text{H}\beta$, resulting in a higher Fe II/ $\text{H}\beta$ ratios together with narrower line width with respect to those observed from an inclined viewing angle (see Figure 1). This explains the anti-correlation between the Fe II/ $\text{H}\beta$ ratio and the $\text{FWHM}(\text{H}\beta)$ [O7]. However, we note that the present model explains only a factor of two difference in the Fe II/ $\text{H}\beta$ ratio while the observed ratio lies in a wider range between $\sim 0.1 - \sim 3$ (e.g., Joly 1991). As mentioned before, the Fe II emitting regions are thought

to be very optically thick. In order to explain the observed range, sophisticated photoionization models will be necessary (see section 7.4).

Another concern is that the present model cannot explain directly why there are NLS1s with both weaker Fe II/ $\text{H}\beta$ ratios and narrower line widths although it explains the anti-correlation [O7]. Here it is again noted that the Fe II emitting regions are expected to be optically very thick. It seems difficult to observe the Fe II emitting regions in some NLS1s even if we see the disk-like BLR from a nearly pole-on view. Alternatively, some NLS1s may have a smaller volume of the partly-ionized region in the BLR. Although we cannot rule out another possibility that a variety in $\text{FWHM}(\text{H}\beta)$ is partly controlled by the mass of SMBHs; i.e., some S1s have lower M_{\bullet} than typical S1s (the low- M_{\bullet} model), it is not necessarily to introduce this idea to explain the observed relationship between the Fe II/ $\text{H}\beta$ ratio and $\text{FWHM}(\text{H}\beta)$.

7.3. The Soft X-ray Emitting Region

In this section we consider where the major emitting region of soft X-ray photons is. Several mechanisms may be responsible for the excess production of soft X-ray emission. It has been often considered that the soft X-ray emission arises from the accretion disk (Madau 1988; Ross, Fabian, & Mineshige 1992; Ross & Fabian 1993). For example, in an optically-thick, geometrically-thin accretion disk, Madau (1988) take the occultation of the innermost disk region due to self-shadowing and the reflection effect of photons off the funnel wall into account and then find that UV and soft X-ray emission is enhanced if we observe this accretion disk from a nearly pole-on view. However, Walter & Fink (1993) suggested that spectral energy dis-

tributions between UV and soft X ray predicted by such accretion disk models appear inconsistent with the observations.

One of very important observational properties of NLS1s related to the soft X-ray emitting region is the discovery of evidence for the relativistic outflow in three NLS1s; 1H 0707–495, IRAS 13224–3809, and PG 1404+226 (Leighly et al. 1997). These outflows are probed by the broad absorption features around 1 keV; the inferred blueshifts lie in a range between $0.2c$ and $0.57c$. In addition to these three, Vaughan et al. (1999) find other three NLS1s (Ton S180, PG 1244+026, and Ark 564) also have such unusual absorption features. Moreover, there are three NLS1s with usual warm absorber (NGC 4051, IRAS 17020+45, and IRAS 20181–22); O VII and O VIII edges at 0.74 and 0.87 keV. In summary, among the 22 NLS1s analyzed by Vaughan et al. (1999), the above nine NLS1s show absorption features. See Iwasawa, Brandt, & Fabian (1998) for the X-ray absorption in one of the strong-Fe II NLS1s, Mrk 507. It is remarkable that the NLS1s with the absorption have narrower H β line widths; an average FWHM $\approx 800 \pm 180$ km s $^{-1}$. On the other hand, the remaining NLS1s have an average FWHM $\approx 1290 \pm 320$ km s $^{-1}$. We examine the difference of the frequency distribution of FWHMs between the NLS1s with absorption features and NLS1s without them. We adopt the null hypothesis that the NLS1s with and without absorption features come from the same underlying distribution. Applying the Kormogrov-Smirnov (KS) statistical test, we obtain the probability of randomly selecting the FWHMs from the same underlying population as 5.4×10^{-5} . Therefore, the difference in FWHM between the two samples appears statistically real. Vaughan et al. (1999) suggested that this property can be understood in terms of the pole-on view model; e.g., if the absorbing material originates in an outflow from the disk, it would only be seen in low inclination systems.

Since relativistic outflows of plasma are expected to produce synchrotron emission in the radio, they may be identical to relativistic radio jets. Indeed, nuclear radio jets have been found in most Seyfert galaxies (e.g., Ulvestad & Wilson 1989). Furthermore, recent detailed morphological studies of inner regions of the NLR in some nearby Seyfert nuclei have shown that the optical NLRs are associated with the radio jet (Bower et al. 1995; Capetti et al. 1995, 1996). These observations have strongly suggested that the NLR associated with the radio jet may be formed by the ionizing fast shock driven by the radio jet rather than the photoionization (Dopita & Sutherland 1995, 1996; Dopita et al. 1997; Bicknell et al. 1998; Falcke, Wilson, & Simpson 1998; Wilson & Raymond 1999; see also Daltabuit & Cox 1972; Wilson & Ulvestad 1983; Norman & Miley 1984). Although it is still uncertain that the majority of the NLR of Seyfert nuclei are formed by the ionizing shock (Laor 1998; Evans et al. 1999), the spatial coincidence between the radio jets and the optical emission-line gas means that the ionizing shock works in part. If the radio jet interacts with the dense ambient gas in very close to the central engine, this can be responsible for the formation of hot plasma, giving rise to the production of X-ray photons; note that the energy of 0.1 keV corresponds to the kinetic temperature $T_{\text{kin}} \simeq 1.16 \times 10^6$ K.

Here we consider what happens when a radio jet interacts with the dense ambient gas following Norman & Miley (1984). The jet is characterized by the jet luminosity L_{jet} , the jet velocity v_{jet} , and the solid opening angle of the jet Ω_{jet} . The pressure exerted on the ambient gas by the radio jet is estimated as

$$p_{\text{jet}} \sim 0.01 \left(\frac{L_{\text{jet}}}{10^{44} \text{ erg s}^{-1}} \right) \left(\frac{\Omega_{\text{jet}}/4\pi}{0.01} \right)^{-1} \times \left(\frac{r_{\text{jet}}}{1 \text{ pc}} \right)^{-2} \left(\frac{v_{\text{jet}}}{10^5 \text{ km s}^{-1}} \right)^{-1} \text{ dyne cm}^{-2}. \quad (6)$$

where r_{jet} is the radial distance of the jet. If we assume that the ambient gas clouds can cool and reach pressure equilibrium in the cocoon of the jet, we obtain a kinetic temperature of the gas

$$T_{\text{kin}} \sim 10^4 \left(\frac{n_e}{10^{10} \text{ cm}^{-3}} \right)^{-1} \left(\frac{L_{\text{jet}}}{10^{44} \text{ erg s}^{-1}} \right) \left(\frac{\Omega_{\text{jet}}/4\pi}{0.01} \right)^{-1} \times \left(\frac{r_{\text{jet}}}{1 \text{ pc}} \right)^{-2} \left(\frac{v_{\text{jet}}}{10^5 \text{ km s}^{-1}} \right)^{-1} \text{ K} \quad (7)$$

where n_e is the electron density. For typical Seyfert nuclei, L_{jet} is of the order of 10^{40} erg s $^{-1}$ at most (e.g., Wilson, Ward, & Haniff 1988). Although large-scale radio jets (i.e., kpc jets) have jet velocities of the order of 10^4 km s $^{-1}$ (e.g., Wilson & Ulvestad 1983; Gallimore, Baum, & O’dea 1996), the inner jet velocities inferred from the broad absorption features in soft X-ray spectra is of the order of 10^5 km s $^{-1}$ (Leighly et al. 1997). An important question is where the soft X-ray emitting region is along the jet. The soft X-ray excess is generally observed in S1s (e.g., Mushotzky, Done, & Pounds 1993). The unified model suggests that the soft X-ray emitting region is hidden by a dusty torus in S2s. Since the typical half height of dusty tori is of the order of 0.1 pc (Taniguchi & Murayama 1998 and references therein), we estimate a typical radial distance of the soft X-ray emitting region is ~ 0.01 pc or less; we thus adopt $r_{\text{jet}} \sim r_{\text{soft X}} \sim 0.01$ pc. This is almost comparable to that of the disk BLR. However, it is noted that the jet develops toward a direction perpendicular to the accretion disk (i.e., to the BLR disk). Therefore, electron densities in such ambient matter may be lower than those in the disk BLR and be similar to those in the warm absorber region (WAR); we thus adopt the typical electron density of the WAR, $\sim 10^8$ cm $^{-3}$ (e.g., Nishiura & Taniguchi 1998 and references therein). Then we obtain a typical kinetic temperature of the jet-driven shocked region

$$T_{\text{kin}} \sim 10^6 \left(\frac{n_e}{10^8 \text{ cm}^{-3}} \right)^{-1} \left(\frac{L_{\text{jet}}}{10^{40} \text{ erg s}^{-1}} \right) \left(\frac{\Omega_{\text{jet}}/4\pi}{0.01} \right)^{-1} \times \left(\frac{r_{\text{soft X}}}{0.01 \text{ pc}} \right)^{-2} \left(\frac{v_{\text{jet}}}{10^5 \text{ km s}^{-1}} \right)^{-1} \text{ K}. \quad (8)$$

This temperature is high enough to produce soft X-ray photons and appears consistent with the estimated black-body temperatures for the NLS1s, ~ 0.1 keV (Pounds et

al. 1995; Puchnarewicz et al. 1995a, 1995b; Vaughan et al. 1999). We note that we can obtain $T_{\text{kin}} \sim 10^6$ K if we adopt $r_{\text{jet}} \sim 0.001$ pc and $n_e \sim 10^{10} \text{ cm}^{-3}$.

We investigate whether or not this idea is responsible for the steep soft X-ray spectra observed in NLS1s. Our model assumes that the excess soft X-ray emission is attributed to the thermal emission made by jet-driven shocks. Therefore, the soft X-ray spectrum is characterized by the black body radiation with $T_{\text{kin}} \sim 10^6$ K. Since the soft X-ray spectra of NLS1s are dominated by the so-called soft excess emission over the underlying power-law continuum (e.g., Vaughan et al. 1999), it seems reasonable to assume that the specific flux in the soft X-ray is described by the Planck function;

$$f_\nu(T) \approx B_\nu(T) = \frac{2h}{c^2} \frac{\nu^3}{e^{h\nu/kT} - 1} \quad (9)$$

where $T \equiv T_{\text{kin}}$. The spectral index at a frequency ν is given by

$$\alpha(\nu, T) = \frac{dB_\nu(T)/d\nu}{B_\nu(T)/\nu} = 3 - \frac{h\nu/kT}{1 - e^{-h\nu/kT}}. \quad (10)$$

Since $f_\nu/(h\nu) \propto \nu^{\alpha-1} \propto E^{-\Gamma}$, the photon index Γ is related to the spectral index as

$$\Gamma(\nu, T) = 1 - \alpha(\nu, T) = \frac{h\nu/kT}{1 - e^{-h\nu/kT}} - 2. \quad (11)$$

Introducing the following parameter

$$x \equiv \frac{h\nu}{kT} = 11.6 \left(\frac{E}{\text{keV}} \right) \left(\frac{T}{10^6 \text{K}} \right)^{-1}, \quad (12)$$

we obtain a relation

$$\frac{T}{10^6 \text{K}} = \frac{11.6}{x} \left(\frac{E}{\text{keV}} \right). \quad (13)$$

In Table 2, we give values of Γ as a function of T at an energy of $E = 1$ keV; i.e., $\Gamma \simeq \Gamma_{\text{soft}}$. It is known that the NLS1s have $\Gamma_{\text{soft}} \simeq 3 - 5$ [X1] (e.g., BBF96). These steeper soft X-ray spectra can be explained if $T_{\text{kin}} \simeq (1.7 - 2.3) \times 10^6$ K. The spectral fitting for 22 NLS1s gives an average kinetic temperature $\bar{T}_{\text{kin}} = (2.00 \pm 0.86) \times 10^6$ K (Vaughan et al. 1999). Therefore our model appears consistent with the observations.

In the above analysis, we assumed that the soft X-ray emitter is at rest. However, the observed absorption features at 1.1 – 1.4 keV imply that the soft X-ray absorbers are moving at velocities of $\sim 0.2c - 0.6c$ [X4]. Taking this point into account, one can obtain

$$\frac{T_{\text{rest}}}{10^6 \text{K}} = \frac{11.6}{x} \left(\frac{E_{\text{obs}}}{\text{keV}} \right) \delta^{-1} \quad (14)$$

where T_{rest} is the kinetic temperature in the rest frame [note that this is the same as T in equation (13)], E_{obs} is the energy in the observed frame, and δ is the kinetic Doppler factor defined by

$$\delta \equiv [\gamma(1 - \beta \cos i_{\text{view}})]^{-1}, \quad (15)$$

where β is the bulk velocity of the emitting region in units of the light speed (i.e., $\beta = v/c$) and $\gamma = (1 - \beta^2)^{-1/2}$ is

the Lorentz factor (e.g., Ghisellini et al. 1993). Given the observed range of β between 0.2 and 0.6, the kinetic temperature of the soft X-ray emitting region can be lowered at most by a factor between 1.1 – 1.6. In Table 3, we give a summary of the photon index at an energy of 1 keV as functions of T_{kin} , β , and i_{view} . It is shown that the observed steep photon indices are obtained within reasonable parameter ranges; $T_{\text{kin}} \simeq (1 - 2) \times 10^6$ K and $\beta \simeq 0.2 - 0.7$.

Another merit of our model is that the relativistic outflows also lead to the enhancement of the soft X-ray luminosity due to the kinematical Doppler effect; i.e.,

$$L_{\text{soft}}^{\text{obs}} = \delta^4 L_{\text{soft}}^{\text{rest}}. \quad (16)$$

Therefore NLS1s viewed from a more pole-on tend to have higher soft X-ray luminosities given a certain relativistic jet velocity. This explains why soft X-ray surveys tend to pick up NLS1s more preferentially. In Table 4, we give numerical values of δ^4 for a various set of both β and i_{view} . It is shown that the luminosity brightening due to the kinematic Doppler factor for the pole-on view is larger by a factor of ≈ 2.08 (1.15) than that for $i_{\text{view}} = 30^\circ$ if $\beta = 0.6$ ($\beta = 0.2$). Therefore, our model suggests that NLS1s have steeper photon indices in the soft X-ray than BLS1s. It is also suggested that NLS1s are systematically brighter in the soft X-ray than BLS1s. All these are consistent with the observations ([X1] and [X2]). NLS1s with both smaller Γ and narrower FWHM($H\beta$) may be either those with higher (or very lower) kinetic temperatures or those with higher-velocity outflows or both. Furthermore, our model appears consistent with the fact that the detection rate of typical WAR is lower in the NLS1s than that in the BLS1s [X4].

We investigate in more detail the important correlation [X2]. First, we consider why S1s with larger FWHM($H\beta$) (i.e., BLS1s) have flatter spectra. Since BLS1s are viewed from intermediate orientations, the brightening due to the kinematic Doppler effect is generally weak. Therefore the soft X-ray excess emission is less dominant than that in NLS1s. We also have to take account that BLS1s with larger FWHM($H\beta$) tend to be observed from more inclined viewing angles if the intrinsic FWHM($H\beta$) is not so different from S1 to S1. Thus, the extinction of soft X-ray photons due to dust grain above the dusty tori are expected to more serious on average for the BLS1s than for the NLS1s. These two orientation effects can be responsible for the flatter soft X-ray spectra of the BLS1s.

Second, we consider why NLS1s with flat soft X-ray spectra. If the jet velocity is not so highly relativistic although the jet can cause shocked regions with $T_{\text{kin}} \sim 10^6$ K, or if the volume of the shocked region is fairly small, the blackbody radiation to the power law continuum luminosity ratio is small. Since the viewing angle dependence due to the kinetic Doppler effect is also small, the soft X-ray spectrum is dominated by the power-law continuum and thus $\Gamma_{\text{soft}} \sim 2$ regardless of FWHM($H\beta$).

Thirdly, we consider why there is a large scatter in Γ_{soft} of the NLS1s. This observed scatter can be attributed either to a variety in T_{BB} (see Table 3) or to the relative predominance of the black body radiation with respect to the power-law continuum or both. In order to investigate

TABLE 2
SOFT X-RAY PHOTON INDICES AS A FUNCTION OF T
AT AN ENERGY OF $E = 1$ KEV

Γ	x^a	T (10^6 K)
1	2.8214	4.11
2	3.9027	2.96
3	4.9651	2.34
4	5.9849	1.94
5	6.9936	1.67

$$^a x \equiv h\nu/(kT).$$

which effect is more important, in Figure 2, we show a diagram between the soft X-ray photon index $\Gamma_{\text{soft}} \equiv \Gamma(0.1 - 2.4 \text{ keV})$ and the black-body to power-law luminosity ratio in the X ray (i.e., $0.6 - 10 \text{ keV}$) for the sample of NLS1s studied by Vaughan et al. (1999) who performed the spectral fitting of the ASCA X-ray spectra using the two components; the black body radiation and the power-law continuum. Here a Hubble constant $H_0 = 50 \text{ km s}^{-1} \text{ Mpc}^{-1}$ and a deceleration parameter $q_0 = 0.5$ are adopted. The black body temperatures estimated by them are shown by filled circles with different colors. Note that a black body temperature of $T_{\text{BB}} = 1.7 \times 10^6 \text{ K}$ is assumed in the fitting for both I Zw 1 and Mrk 507 because of relatively poor S/N of the spectra (Vaughan et al. 1999). We construct two-component models in which the black body radiation and the power-law continuum are taken into account. Here we adopt the canonical hard X-ray photon index for NLS1s $\Gamma_{\text{hard}} = 2.1$ (Vaughan et al. 1999) for the power-law continuum. Our model results are also shown in Figure 2 by thick curves as a function of T_{BB} . Although the spectral fitting by Vaughan et al. (1999) leads to a variety of T_{BB} by a factor of three [i.e., $T_{\text{BB}} \simeq (1 - 3) \times 10^6 \text{ K}$], our model results suggest that the majority of the NLS1s have $T_{\text{BB}} \simeq (0.7 - 1) \times 10^6 \text{ K}$. Although these values are slightly lower than our previous estimates based on Table 3 [i.e., $T_{\text{BB}} \simeq (1 - 2) \times 10^6 \text{ K}$], this slight difference is due to that our previous estimates do not include the contribution of the power-law continuum. It is likely that $L_{\text{BB}}/L_{\text{PL}}$ seems to be evaluated more accurately than T_{BB} in the spectral fitting by Vaughan et al. (1999) because L_{BB} is estimated by integrating the soft excess emission while the estimate of T_{BB} is sensitive to the peak in the soft X-ray part of the spectra which has often poorer S/N. Therefore, the observed scatter in Γ_{soft} of the NLS1s is attributed mainly to the relative predominance of the black body radiation.

Here a question arises as what determines the black body temperature. Since the origin of the black body radiation is attributed to the jet-driven shocks in our model, the temperature is determined by the ratio between the mechanical luminosity of the jet and the gas mass of the shocked region if we neglect the relativistic effect of the jet velocity. In Figure 3, we show a diagram between Γ_{soft} and the soft X-ray luminosity to the radio jet power at $\lambda = 6$

cm for the Vaughan et al.'s (1999) NLS1 sample. The radio continuum data are taken from Ulvestad et al. (1995). The data set is too small to obtain any statistically significant results. However, it is interesting to see a trend that NLS1 with steeper Γ_{soft} have higher $L_{\text{soft}}/P_{\text{jet}}$ ratios [see also Figure 9 in Walter & Fink (1993)]. This tendency may be interpreted by that NLS1s with a lot of dense ambient gas have higher soft X-ray luminosities because of relatively larger volume of the shocked region but the temperature of the shocked region does not increase significantly, giving rise to steeper Γ_{soft} . Unfortunately, the black body temperature is available only for three NLS1s. In order to verify this possibility, more sensitive, soft and hard X-ray spectroscopy as well as deep radio-continuum mapping for a larger sample of S1s will be recommended. In Figure 4, we also show a diagram between Γ_{soft} and L_{soft} for the NLS1s studied by BBF96 (upper panel) and the S1s (NLS1s + BLS1s) studied by Walter & Fink (1993) (lower panel). It is shown that there is a clear, positive correlation only for the NLS1s; its correlation coefficient is 0.66. This implies that NLS1s with higher L_{soft} have a larger volume of the shocked region but have a lower black body temperature; note that the soft X-ray luminosity due to the black body radiation is estimated to be $L_{\text{soft}}(\text{BB}) = 4\pi r^2 \sigma T_{\text{BB}}^4$ where σ is the Stephan-Boltzmann constant if the shocked region has a spherical form with a radius of r .

Finally we mention about a typical size of the soft X-ray emitting regions. The variability timescale observed in the soft X ray is of the order of one day or less (BBF96), corresponding to a linear size of $\sim 3 \times 10^{15} \text{ cm} \sim 0.001 \text{ pc}$. The soft X-ray emitting region is located at a distance of $\sim 0.01 \text{ pc}$ from the central engine in our model. However, the above timescale suggests that a typical size of the soft X-ray emitting region is as small as $\sim 0.001 \text{ pc}$. As mentioned before, we have an alternative option; the soft X-ray emitting region is located at a distance of $\sim 0.001 \text{ pc}$ from the central engine and a typical size of the soft X-ray emitting region is also as small as $\sim 0.001 \text{ pc}$.

7.4. A New Photoionization Scenario for the Disk-like Broad Line Region

TABLE 3
 THE PHOTON INDEX AT 1 KEV AS FUNCTIONS OF T_{kin} , β , AND i_{view}

β	i_{view} ($^{\circ}$)	δ	$\Gamma(1 \text{ keV})$				
			$T_{\text{kin}} (10^6 \text{ K})$				
			1.0	2.0	3.0	4.0	5.0
0.0	...	1.000	9.61	3.82	1.95	1.07	0.57
0.1	0	1.106	8.50	3.28	1.61	0.83	0.39
0.2	0	1.225	7.48	2.78	1.30	0.61	0.23
0.3	0	1.363	6.52	2.32	1.01	0.42	0.08
0.4	0	1.528	5.60	1.89	0.75	0.23	-0.05
0.5	0	1.732	4.71	1.47	0.50	0.06	-0.18
0.6	0	2.000	3.82	1.07	0.26	-0.11	-0.31
0.7	0	2.380	2.91	0.67	0.02	-0.27	-0.43
0.8	0	3.000	1.95	0.26	-0.22	-0.44	-0.56
0.9	0	4.359	0.86	-0.19	-0.49	-0.63	-0.71
0.1	5	1.105	8.50	3.28	1.61	0.83	0.39
0.2	5	1.224	7.48	2.78	1.30	0.62	0.23
0.3	5	1.361	6.53	2.33	1.02	0.42	0.08
0.4	5	1.524	5.62	1.89	0.76	0.24	-0.05
0.5	5	1.725	4.73	1.48	0.51	0.07	-0.18
0.6	5	1.989	3.85	1.08	0.27	-0.10	-0.31
0.7	5	2.360	2.95	0.69	0.03	-0.26	-0.43
0.8	5	2.955	2.01	0.28	-0.21	-0.43	-0.56
0.9	5	4.215	0.94	-0.16	-0.47	-0.62	-0.70
0.1	10	1.104	8.51	3.28	1.61	0.83	0.40
0.2	10	1.220	7.51	2.80	1.31	0.62	0.24
0.3	10	1.354	6.57	2.35	1.03	0.43	0.09
0.4	10	1.512	5.68	1.92	0.77	0.25	-0.04
0.5	10	1.706	4.81	1.52	0.53	0.08	-0.17
0.6	10	1.955	3.95	1.13	0.30	-0.08	-0.29
0.7	10	2.299	3.08	0.74	0.07	-0.24	-0.41
0.8	10	2.828	2.17	0.35	-0.16	-0.40	-0.53
0.9	10	3.835	1.18	-0.06	-0.41	-0.57	-0.67
0.1	20	1.098	8.57	3.31	1.63	0.84	0.40
0.2	20	1.207	7.62	2.85	1.34	0.64	0.25
0.3	20	1.328	6.74	2.42	1.08	0.46	0.12
0.4	20	1.468	5.91	2.03	0.84	0.29	-0.01
0.5	20	1.634	5.11	1.66	0.61	0.14	-0.13
0.6	20	1.834	4.34	1.30	0.40	-0.01	-0.24
0.7	20	2.087	3.58	0.96	0.20	-0.15	-0.34
0.8	20	2.417	2.84	0.64	0.01	-0.28	-0.44
0.9	20	2.825	2.18	0.36	-0.16	-0.40	-0.53
0.1	30	1.089	8.65	3.35	1.66	0.86	0.42
0.2	30	1.185	7.79	2.93	1.39	0.68	0.28
0.3	30	1.289	7.01	2.55	1.16	0.52	0.16
0.4	30	1.402	6.28	2.20	0.95	0.37	0.05
0.5	30	1.527	5.60	1.89	0.75	0.23	-0.05
0.6	30	1.665	4.97	1.59	0.58	0.11	-0.15
0.7	30	1.814	4.41	1.34	0.42	0.00	-0.23
0.8	30	1.953	3.96	1.13	0.30	-0.08	-0.29
0.9	30	1.976	3.89	1.10	0.28	-0.09	-0.30

TABLE 4
 THE LUMINOSITY BRIGHTENING FACTOR (δ^4) DUE TO THE KINEMATIC DOPPLER EFFECT
 AS FUNCTIONS OF β AND i_{view}

β	δ^4				
	$i_{\text{view}} = 0^\circ$	$i_{\text{view}} = 5^\circ$	$i_{\text{view}} = 10^\circ$	$i_{\text{view}} = 20^\circ$	$i_{\text{view}} = 30^\circ$
0.1	1.494	1.491	1.484	1.454	1.408
0.2	2.250	2.241	2.216	2.119	1.972
0.3	3.449	3.427	3.361	3.114	2.759
0.4	5.444	5.390	5.229	4.650	3.867
0.5	9.000	8.864	8.473	7.121	5.443
0.6	16.00	15.64	14.62	11.32	7.691
0.7	32.11	31.00	27.93	18.96	10.82
0.8	81.00	76.25	63.97	34.13	14.56
0.9	361.0	315.5	216.2	63.72	15.25

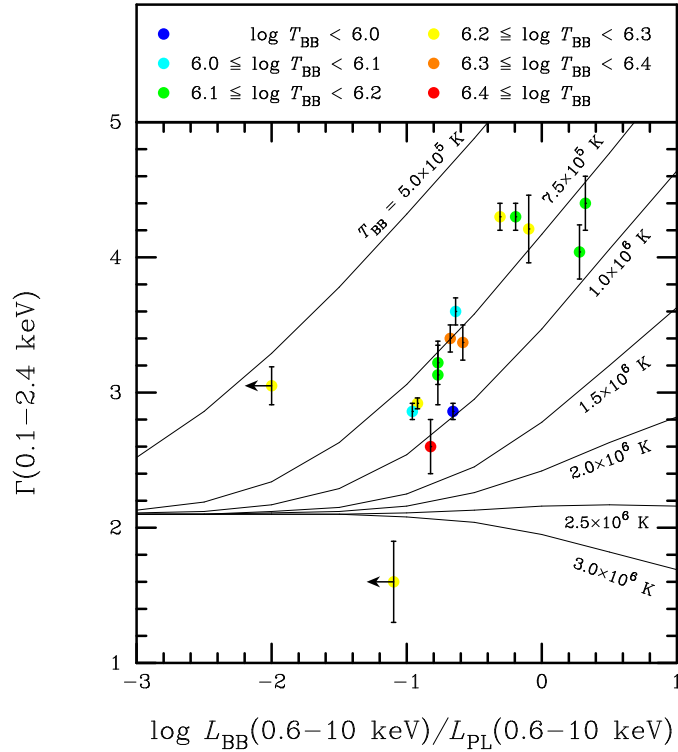


FIG. 2.— A diagram between the soft X-ray photon index Γ_{soft} and the black-body to power-law luminosity ratio in the X ray (i.e., 0.6 – 10 keV) for the sample of NLS1s studied by Vaughan et al. (1999). The black body temperatures estimated by them are shown by filled circles with different colors (see the upper panel). Our model results by thick curves as a function of T_{BB} in which the canonical hard X-ray photon index for NLS1s is adopted to be 2.1 (Vaughan et al. 1999).

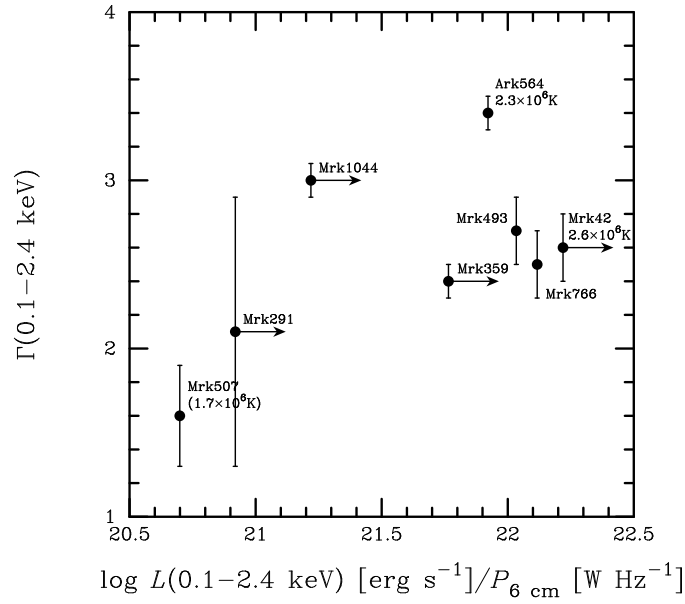


FIG. 3.— A diagram between Γ_{soft} and the soft X-ray luminosity to the radio jet power at $\lambda = 6$ cm for the Vaughan et al.'s (1999) NLS1 sample.

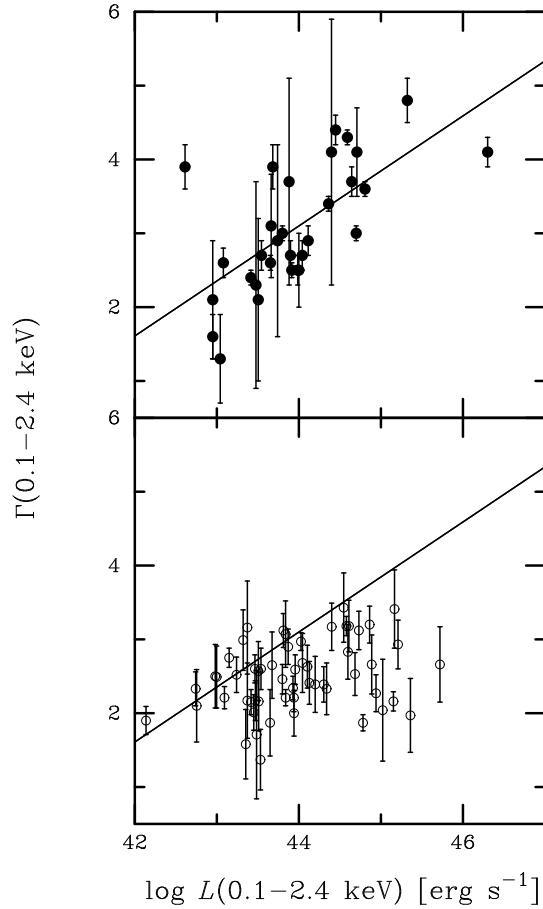


FIG. 4.— A diagram between Γ_{soft} and L_{soft} for the NLS1s studied by BBF96 (upper panel) and S1s studied by Walter & Fink (1993) (Lower panel).

We have described the pole-on view model is responsible for the two important correlations, [O7] (section 7.2) and [X2] (section 7.3). In this section, we investigate how these two correlations are linked physically.

It is widely accepted that the BLR is photoionized by the nonthermal continuum from the central engine although shock heating models are also sometimes discussed (e.g., Rees 1984; Blandford 1990). As discussed in section 7.2, optically-thick, partly ionized regions from which the Fe II emission arises are mainly heated by X-ray photons (Ferland & Netzer 1979; Kwan & Krolik 1981). High energy photons formed by the synchrotron self Compton effect are associated with relativistic outflows and thus are thought to be highly beamed. The direction of the beaming is believed to be perpendicular to the accretion disk. Therefore, it is unlikely that these high energy photons are responsible for the ionization of the disk-like BLR. Indeed Wang et al. (1996) showed that NLS1s with strong Fe II emission have lower X-ray luminosities at 2 keV and thus suggested that the Fe II emitting region cannot be heated by X rays with energies of ~ 2 keV. Instead, the optically-thick accretion disk around a supermassive compact object is also thought to play an important role in the ionization of the disk-like BLR. The optically-thick condition leads to that gas particles dissipate their energy locally because of the viscosity. In this case, we can approximate the local emission as blackbody. Since the accretion disk has a temperature gradient, superposition of such blackbody emission with various temperatures can mimic to the power-law like continuum emission. The temperature of such an accretion disk around a Schwarzschild supermassive black hole can be written as

$$T(r) \approx 2.8 \times 10^5 (\dot{M}/\dot{M}_{\text{Edd}}) M_{\bullet,8}^{-1/4} [r/(3r_S)]^{-3/4} \text{ K} \\ (\text{for } r \geq 3r_S), \quad (17)$$

where \dot{M} is the accretion rate, \dot{M}_{Edd} is the Eddington accretion rate, $M_{\bullet,8}$ is the black hole mass in units of $10^8 M_{\odot}$, and r_S is the Schwarzschild radius (e.g., Peterson 1997). Therefore, this radiation is mainly emitted in the UV region, responsible for the photoionization of the disk-like BLR. However, since this continuum emission does not contain a lot of higher energy photons, it is unlikely that this continuum creates a huge volume of partly ionized regions in the disk-like BLR (see upper panel of Figure 6). Therefore, it is expected that a dense gas cloudlet immersed in the disk-like BLR consists of both a fully-ionized zone facing to the continuum and a neutral zone. This means that Fe II emission cannot arise from this cloudlet efficiently.

As shown in Figure 4, there is the clear correlation between Γ_{soft} and the soft X-ray luminosity. In addition, Wang et al. (1996) showed that there is a positive correlation between Γ_{soft} and the Fe II $\lambda 4570/\text{H}\beta$ ratio. The simplest interpretation for these correlations is that the stronger Fe II emission is attributed to the soft X-ray excess emission; i.e., Fe II emitting regions in the disk-like BLR are photoionized by the soft X-ray excess emission. We have shown that jet-driven shocks lead to the formation of hot regions with $T_{\text{kin}} \simeq 10^6$ K. Since this emission is approximated by the blackbody radiation, soft X-ray photons are emitted isotropically; note, however, that the

shocked region are thought to be moving a relativistic velocity and thus the radiation field is modulated by this effect. These soft X-ray photons irradiate the disk-like BLR. The outer surfaces of cloudlets in the disk-like BLR are photoionized by these photons. If these cloudlets are ionization-bounded, there are neutral regions inside the cloudlets. Since some high energy photons can penetrate into the inner regions, it is expected that partly ionized regions are made there. In Figure 5, we show a diagram between the Fe II/H β ratio and the black-body radiation to power-law continuum luminosity ratio in the hard X ray which is estimated by Vaughan et al. (1999). Although the data points show a large scatter, there is a marginal tendency that NLS1s with larger Fe II/H β ratios tend to have higher $L_{\text{BB}}/L_{\text{PL}}$ ratios. We thus propose that this is the formation mechanism of the Fe II emitting region in the disk-like BLR (see lower panel of Figure 6). Although we are not going to give more detailed photoionization modeling, the new idea presented here appears to explain the origin of the Fe II emitting region qualitatively.

7.5. Confrontation with Observation

Our new model was constructed to explain the two most important correlations; between the Fe II/H β intensity ratio and the FWHM(H β) [O7] and between the soft X-ray photon index Γ and the FWHM(H β) [X2]. Although these two correlations are explained by the viewing angle dependence without invoking other mechanisms, there are a number of other important observational properties of NLS1s summarized in section 2. Therefore, in this section, we investigate whether or not our new model is also consistent with them.

The equivalent widths of Balmer lines of NLS1s are on average lower by a factor of ≈ 2 than those of BLS1s [O3]. This is consistently explained by the difference of the average viewing angle between the NLS1s and the BLS1s if the optical continuum emission arises mainly from the optically-thick accretion disk. The optical polarization of NLS1s is interpreted by the dust scattering [O9]. This may be caused either at the inner wall of dusty tori or the dusty NLR clouds (Netzer & Laor 1993; Wolf & Henning 1999). Robinson (1995) suggested that the profiles of BLR emission of NLS1s are generally different from those of BLS1; i.e., a normal broad-line profile has a more dominant core than a NLS1 profile [O2]. Since there are two kinds of BLR (i.e., a disk-like and a jet-like BLR in a Seyfert galaxy), it is expected that the relative contribution of these two components to the total flux may be different from Seyfert to Seyfert. Therefore, it may not be surprising to observe various kinds of Balmer emission-line profiles. The anti-correlation between Fe II $\lambda 4570/\text{H}\beta$ and [O III] $\lambda 5007/\text{H}\beta$ [O8] can be understood if the NLR has a significant amount of dust grains (Netzer & Laor 1993) because the NLS1s are viewed from lower viewing angles and thus the effect of extinction on the [O III] emission could be more serious than that for the BLS1s.

Since the HI-BLR emission lines are thought to arise from the jet-like BLR, there can be little difference in the UV emission line properties ([U1] and [U2]) between the NLS1s and the BLS1s. Since the UV – soft X-ray emitting regions in NLS1s are moving toward us at relativistic velocities, the UV part of the continuum emission is

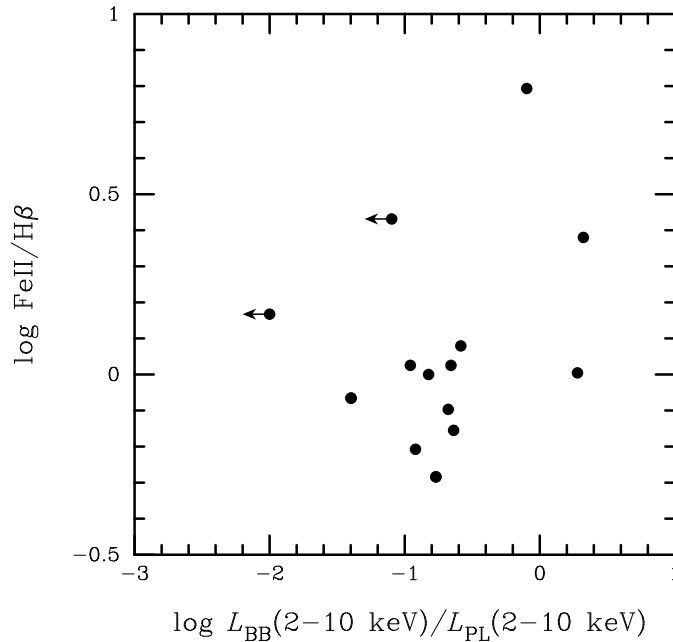


FIG. 5.— A diagram between the Fe II/H β ratio and the black-body radiation to power-law continuum luminosity ratio in the hard X ray which is estimated by Vaughan et al. (1999).

blueshifted to the soft X-ray regime and thus the UV luminosities of NLS1s are expected to be less luminous than those of BLS1s systematically [U3]. This effect may also contribute to the softer hard X-ray spectra observed in NLS1s [X3].

Walter & Fink (1993) found the positive correlation between Γ_{soft} and the UV (1375 Å)-to-X ray (2 keV) flux ratio for S1s and NLS1s follow this correlation [X8]. In our model the UV continuum is mainly supplied by the optically-thick accretion disk. In order to explain this correlation, it will be necessary to construct a more general model including the accretion disk emission.

It is worth noting the radio continuum image of one of NLS1s, Mrk 766 (Ulvestad et al. 1995). Since this NLS1 is a very nearby object, this is fortunately resolved spatially in the 3.6 cm and 6 cm radio continuum maps. The linear size is 60 pc although the shape is slightly elongated in position angle of $12^\circ \pm 5^\circ$. A typical linear size of the radio jets in BLS1s is 350 pc (Ulvestad & Wilson 1989). If the small radio size of Mrk 766 is attributed to the inclination effect, we obtain a viewing angle toward the jet is $i_{\text{view}} = \sin^{-1}(60/350) \approx 10^\circ$, being consistent with those derived from the kinematical and statistical considerations. Since most NLS1s are not resolved in the observations of Ulvestad et al. (1995), the pole-on view model appears consistent with the radio observations in this respect [R2]. However, the following observations are not interpreted easily; two NLS1s (Mrk 766 and Mrk 1126) have radio major axes perpendicular to the optical polarization while the remaining one (Mrk 957) has a radio major axis parallel to the optical polarization [R3]. It has been shown that the optical polarization position angles tend to align with the radio-jet structure in type 1 AGN while be perpendicular to the radio-jet structure in type 2 AGN (Antonucci 1983, 1984, 1992). If NLS1s belong to a subclass of S1s, we would obtain that all the above three NLS1s have radio major axes parallel to the optical polarization.

As mentioned in section 5.2 briefly, accretion disks in AGNs have been probed by the very broad Fe K α emission (Tanaka et al. 1995; Fabian et al. 1995; Mushotzky et al. 1995; Iwasawa et al. 1996; Nandra et al. 1997; Reynolds 1997). Nandra et al. (1997) presented a systematic analysis of the hard X-ray spectra of 18 BLS1s. They fitted the Fe K α emission profiles and derived the most probable inclination angles; $i_{\text{view}} \simeq 29^\circ \pm 3^\circ$. Although these estimates are subject to a number of fitting parameters, it is interesting to note that most of the BLS1s are viewed from such intermediate viewing angles.

7.6. Comments on the GBHC Model

It has been often claimed that the soft excess emission in NLS1s is similar to the observational property of the high state of Galactic black hole candidates (GBHCs) like Cyg X-1 (Tanaka 1990; Pounds et al. 1995; Hayashida 1997). These GBHCs are known to show a dramatic change in spectral shape from a normal AGN-like power law to a state where the soft X-ray emission dominates, perhaps being attributed to the thermal emission from the accretion disk. Although the power-law spectrum can still be seen in this high state, it is often observed to be steeper than before as a result of the increased electron cooling from the enhanced soft X-ray photons. This spectral change may be caused by an increase in the accretion rate; the accretion rates in the GBHCs are thought to be close to the Eddington limit. However, as discussed in section 7.3, the soft X-ray luminosities of NLS1s are extrinsically more enhanced by the kinematical Doppler factor than those of BLS1s. Therefore, it is not necessary to interpret that NLS1s have higher gas accretion rates than BLS1s.

BBF96 also noted the following difficulty for the GBHC model; GBHCs tend to be less variable while in their ultra soft states, while NLS1s do not show reduced variability.

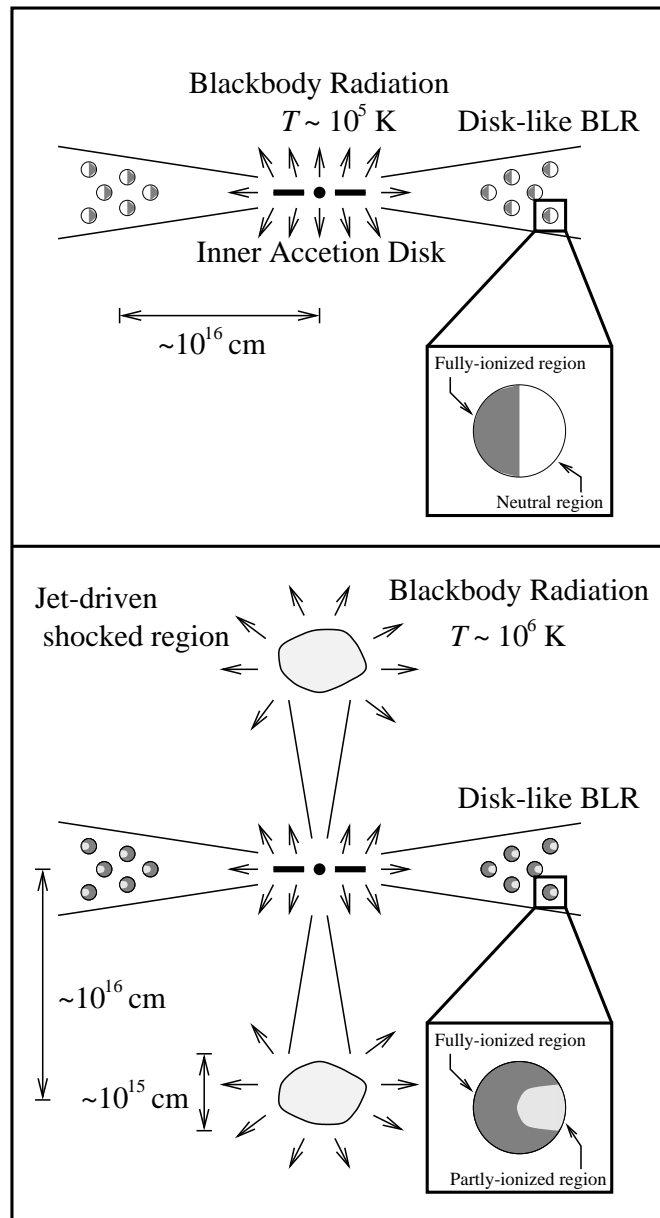


FIG. 6.— Upper panel: Photoionization of cloudlets in the disk-like BLR by the UV continuum emission from the inner accretion disk. Lower panel: Photoionization of cloudlets in the disk-like BLR by the additional soft X-ray sources, giving rise to the formation of partly ionized regions.

8. A VIEWING-ANGLE-DEPENDENT UNIFIED MODEL FOR SEYFERT GALAXIES

8.1. The Critical Viewing Angle to NLS1s

As discussed in section 5.3, the pole-on view model implies that the observed narrow FWHMs of NLS1s are attributed to smaller viewing angles toward the BLR. A critical viewing angle toward NLS1s is $i_{\text{cr,NLS1}} \simeq \sin^{-1}(1000 \text{ km s}^{-1}/12000 \text{ km s}^{-1}) \simeq 4.8^\circ$ or $i_{\text{cr,NLS1}} \simeq 9.6^\circ$ if we adopt the maximum value of $\text{FWHM}(\text{BLR}) = 2000 \text{ km s}^{-1}$ for NLS1s (Vaughan et al. 1999). Since S1s with $\text{FWHM}(\text{BLR}) \simeq 2000 \text{ km s}^{-1}$ are often classified as NLS1s, the latter viewing angle seems a more appropriate estimate. Therefore, we adopt $i_{\text{cr,NLS1}} \simeq 10^\circ$.

8.2. The Critical Viewing Angle to BLS1s

After introducing the dusty torus model for Seyfert nuclei (Antonucci & Miller 1985), many arguments have been made to estimate the critical viewing angle between S1s and S2s (Osterbrock & Shaw 1988; Salzer 1989; Miller & Goodrich 1990; Huchra & Burg 1992; Pogge 1989; Wilson & Tsvetanov 1994; Schmitt & Kinney 1996; Murayama et al. 2000).

a) The statistical method: The critical viewing angle $i_{\text{cr,BLS1}}$ can be estimated from the number statistics of S1s and S2s if we observe Seyfert nuclei from random orientations on the statistical ground,

$$\frac{N_{\text{S1}}}{N_{\text{S1}} + N_{\text{S2}}} = 1 - \cos i_{\text{cr,S1}}(\text{stat}), \quad (18)$$

where N_{S1} and N_{S2} are the observed numbers of S1s and S2s, respectively (Miller & Goodrich 1990). The three different optical surveys of Seyfert galaxies give the following critical angles; $i_{\text{cr,BLS1}}(\text{stat}) \simeq 27^\circ$ (Osterbrock & Shaw 1988), 34° (Salzer 1989), and 46° (Huchra & Burg 1992).

b) The opening angle of NLR: The NLR of S2s often exhibits conical morphologies, which are due to shadowing of the nuclear ionizing continuum by the torus. The observed semi-opening angle of the cone $\theta_{\text{open}}(\text{NLR})$ is thereby equal to the semi-opening angle of the torus θ_{open} as noted in section 6.2 briefly. This angle can be close to the critical viewing angle to BLS1s. The statistical results from observations of conical NLRs give the following opening angle; $\theta_{\text{open}}(\text{NLR}) = 26^\circ \pm 11^\circ$ (Pogge 1989), $32^\circ \pm 8^\circ$ (Wilson & Tsvetanov 1994), and $29^\circ \pm 9^\circ$ (Schmitt & Kinney 1996).

c) The mid-infrared diagnostic: Since the L -band ($3.5 \mu\text{m}$)-to-IRAS $25 \mu\text{m}$ flux ratio is sensitive to the orientation of dusty tori, this ratio can be used to estimate the viewing angle to the dusty tori although dusty torus models are necessary to perform this analysis (Taniguchi et al. 1997; Murayama et al. 2000). Murayama et al.

(2000) found that the critical viewing angle toward BLS1s is about 45° .

In summary, the critical viewing angle to BLS1s lies in a range between 30° and 45° . Since the opening angle of the NLR provides only a direct estimate, we adopt $i_{\text{cr,BLS1}} \simeq 30^\circ$.

8.3. The Critical Viewing Angle to S2s with the Hidden BLR

S2s are also classified into the following two classes; 1) S2s with the hidden BLR (hereafter S2^+), and 2) S2s without the hidden BLR (hereafter S2^-) (e.g., Miller & Goodrich 1990; Tran 1995). Now let us assume that the S2^+ s are viewed at an angle intermediate between S1s and S2^- s (Heisler, Lumsden, & Bailey 1997). We can estimate a critical viewing angle which distinguishes S2^+ from S2^- ($i_{\text{cr,S2}^+}$),

$$\frac{N_{\text{S1}} + N_{\text{S2}^+}}{N_{\text{S1}} + N_{\text{S2}}} = 1 - \cos i_{\text{cr,S2}^+}. \quad (19)$$

Using this relation together with the observed number ratio between S2^+ and S2^- , $N_{\text{S2}^+}/N_{\text{S2}^-} = 10/40 = 0.25$, Taniguchi & Anabuki (1999) obtained $i_{\text{cr,S2}^+} \approx 50^\circ$. This means that Seyfert galaxies viewed from $50^\circ \lesssim i_{\text{view}} \leq 90^\circ$ are identified as S2^- s.

8.4. Summary

The above arguments lead us to propose a viewing-angle-dependent unified model for Seyfert nuclei; 1) $0^\circ \leq i_{\text{view}} \lesssim 10^\circ$ for NLS1s, 2) $10^\circ \lesssim i_{\text{view}} \lesssim 30^\circ$ for BLS1s, 3) $30^\circ \lesssim i_{\text{view}} \lesssim 50^\circ$ for S2^+ s, and 4) $50^\circ \lesssim i_{\text{view}} \leq 90^\circ$ for S2^- s. This is schematically illustrated in Figure 7.

Finally, it seems important to note that the NLS1 phenomenon is also observed in some radio-quiet quasars (Laor et al. 1994, 1997; Fiore et al. 1998; Xu et al. 1999). Therefore, it is strongly suggested that the class of NLS1s is the radio-quiet equivalent of the class of Blazars in radio-loud AGN (see for unified models for radio-loud AGN, Urry & Padovani 1995).

We would like to thank Kazushi Iwasawa, Neil Brandt, Hisamitsu Awaki, and Kiyoshi Hayashida for useful discussion on the X-ray properties of Seyfert nuclei and Hideaki Mouri and Deborah Dultzin-Hacyan for useful discussion on AGN. We also thank our colleagues, Shingo Nishiura, Hiroshi Sudou, and Naohisa Anabuki for useful discussion during the course of this work. TM is a JSPS fellow. This work was financially supported in part by Grant-in-Aids for the Scientific Research (Nos. 10044052, and 10304013) of the Japanese Ministry of Education, Culture, Sports, and Science.

REFERENCES

- Antonucci, R. 1983, *Nature*, 303, 158
Antonucci, R. 1984, *ApJ*, 278, 499
Antonucci, R. 1992, in *Testing the AGN Paradigm*, Eds. Holt, S. S., Neff, S. G., Urry, C. M. (American Institute of Physics: New York), 486
Antonucci, R. 1993, *ARA&A*, 31, 473
Antonucci, R., & Miller, J. S. 1985, *ApJ*, 297, 621
Awaki, H., Koyama, K., Inoue, H., & Halpern, J. P. 1991, *PASJ*, 43, 195
Bicknell, G. V., Dopita, M. A., Tsvetanov, Z. I., & Sutherland, R. S. 1998, *ApJ*, 495, 680
Binette, L. 1985, *A&A*, 143, 334
Blandford R. D. 1990, *Active Galactic Nuclei*, eds. R.D. Blandford, H. Netzer, A. Woltier (Springer-Verlag), 161
Boller, T., Brandt, W. N., & Fink, H. 1996, *A & A*, 305, 53 (BBF96)
Boroson, T. A., & Green, R. F. 1992, *ApJS*, 80, 109
Bower, G. A., Wilson, A. S., Morse, J. A., Geldermann, R., Whittle, M., & Mulchaey, J. S. 1995, *ApJ*, 454, 106

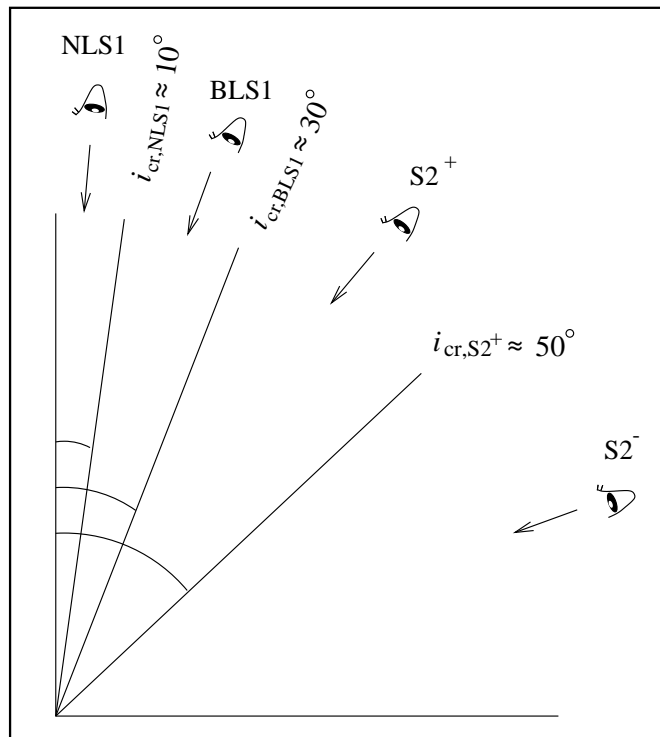


FIG. 7.— A viewing-angle-dependent unified model for Seyfert galaxies (NLS1, BLS1, S2⁺, and S2⁻).

- Brandt, W. N., Mathur, S., & Elvis, M. 1997, MNRAS, 285, L25
- Capetti, A., Axon, D. J., Macchetto, F., Sparks, W. B., & Boksenberg, A. 1996, ApJ, 469, 554
- Capetti, A., Macchetto, F. D., Axon, D. J., Sparks, W. B., & Boksenberg, A. 1995, ApJ, 448, 600
- Collin-Souffrin, S., Hameury, J. -M., & Joly, M. 1988, A&A, 205, 19
- Collin-Souffrin, S., & Lasota, J. -P. 1988, PASP, 100, 1041
- Crenshaw, M. D., Peterson, B. M., Korista, K. T., Wagner, R. M., & Aufdenberg, J. P. 1991, AJ, 101, 1022
- Daltabuit, E., & Cox, D. 1972, ApJ, 173, L13
- Davidson, M. L., & Kinman, T. D. 1978, ApJ, 225, 766
- Dopita, M. A., Koratkar, A. P., Allen, M. G., Tsvetanov, Z. I., Ford, H. C., Bicknell, G. V., & Sutherland, R. S. 1997, ApJ, 490, 202
- Dopita, M. A., & Sutherland, R. S. 1995, ApJ, 455, 468
- Dopita, M. A., & Sutherland, R. S. 1996, ApJS, 102, 161
- Dultzin-Hacyan, D., Taniguchi, Y., & Uranga, L. 1999, Structure and Kinematics of Quasar Broad Line Regions, Eds. C. M. Gaskell, W. N. Brandt, M. Eracleous, M. Dietrich, Dultzin-Hacyan, D., ASP Conf. Ser., 175, 303
- Edelson, R., Vaughan, S., Warwick, R., Puchnarewicz, E. M., & George, I. 1999, MNRAS, 307, 91
- Eracleous, M., & Halpern, J. P. ApJS, 90, 1
- Evans, I., Koratkar, A., Allen, M., Dopita, M., & Tsvetanov, Z. 1999, ApJ, 521, 531
- Fabian, A. C., Nandra, K., Reynolds, C. S., Brandt, W. N., Otani C., Tanaka, Y., Inoue, H., Iwasawa, K. 1995, MNRAS 277, L11
- Falcke, H., Wilson, A. S., & Simpson, C. 1998, ApJ, 502, 199
- Ferland, G. J., & Netzer, H. 1979, ApJ, 229, 274
- Ferland, G. J., & Persson, S. E. 1989, ApJ, 347, 656
- Fiore, F., et al. 1998, MNRAS, 298, 013
- Gallimore, J. F., Baum, S. A., & O'Dea, C. P. 1996, ApJ, 464, 198
- Ghisellini, G., Padovani, P., Celotti, A., & Maraschi, L. 1993, ApJ, 407, 65
- Giannuzzo, M. E., & Stripe, G. M. 1996, A&A, 314, 419
- Giannuzzo, M. E., Mignoli, M., Stripe, G. M., & Comastri, A. 1998, A&A, 330, 894
- Goodrich, R. W., 1989, ApJ, 342, 224
- Greenhill, L., Gwinn, C. R., Antonucci, R., & Barvanis, R. 1996, ApJ, 472, L21
- Grupe, D., Leighly, L. M., Thomas, H. -C., Laurent,-Muehleisen, S. A., 1999, A&A, submitted
- Guilbert, P. W., Fabian, A. C., & McCray, R. 1983, ApJ, 266, 466
- Halpern, J. P., & Oke, J. B. 1987, ApJ, 312, 91
- Hayashida, K. 1997, Emission Lines in Active Galaxies: New Methods and Techniques, eds. B. M. Peterson, F. -Z. Cheng, & A. S., Wilson, ASP Conf., Ser., 113, 40
- Hayashida, K., Miyamoto, S., Kitamoto, S., Negoro, H., & Inoue, H. 1998, ApJ, 500, 642
- Heisler, C. A., Lumsden, S. L., & Bailey, J. A. 1997, Nature, 385, 700
- Huchra, J., & Burg, R. 1992, ApJ, 393, 90
- Iwasawa, K., Brandt, W. N., & Fabian, A. C. 1998, MNRAS, 293, 251
- Iwasawa K., et al. 1996, MNRAS 282, 1038
- Joly, M. 1989, A&A, 208, 47
- Joly, M. 1991, A&A, 242, 49
- Khachikian, E. Ye., & Weedman, D. W. 1974, ApJ, 192, 581
- Koratkar, A. P. & Gaskell, C. M. 1991, ApJ, 370, L61
- Kormendy, J., Bender, R., Evans, A. S., & Richstone, D. 1998, AJ, 115, 1823
- Koski, A. T. 1978, ApJ, 223, 56
- Kraemer, S. B., Crenshaw, D. M., Filippenko, A. V., & Peterson, B. M. 1998, ApJ, 499, 719
- Kwan, J., & Krolik, J. H. 1981, ApJ, 250, 478
- Laor, A. 1998, ApJ, 496, L71
- Laor, A., Fiore, F., Elvis, M., Wilkes, B. J., & McDowell, J. C. 1994, ApJ, 435, 611
- Laor, A., Fiore, F., Elvis, M., Wilkes, B. J., & McDowell, J. C. 1997, ApJ, 477, 93
- Lawrence, A., Elvis, M., Wilkes, B. J., McHardy, I., & Brandt, N. 1997, MNRAS, 285, 879
- Leighly, K. M. 1999a, ApJS, in press (astro-ph/9907294)
- Leighly, K. M. 1999b, ApJS, in press (astro-ph/9907295)
- Leighly, K. M., Mushotzky, R., Nandra, K., & Forster, K. 1997, ApJ, 489, L25
- Madau, P. 1988, ApJ, 327, 116
- Marziani, P., Sulentic, J. W., Dultzin-Hacyan, D., Calvani, M., & Moles, M. 1996, ApJS, 104, 37
- Mason, K. O., Puchnarewicz, E. M., & Jones, L. R. 1996, MNRAS, 283, L26
- Miller, J. S., & Goodrich, R. W. 1990, ApJ, 355, 456
- Miyoshi, M., Moran, J., Herrnstein, J., Greenhill, L., Nakai, N., Diamond, P., & Inoue, M. 1995, Nature, 373, 127
- Murayama, T., Mouri, H., & Taniguchi, Y. 2000, ApJ, 528, in press (astro-ph/9908259)
- Murayama, T., Nagao, T., Taniguchi, Y., & Mouri, H. 1999, in preparation
- Murayama, T., & Taniguchi, Y. 1998a, ApJ, 497, L9
- Murayama, T., & Taniguchi, Y. 1998b, ApJ, 503, L115
- Murayama, T., Taniguchi, Y., & Iwasawa, K. 1998, AJ, 115, 460
- Mushotzky, R. F., Done, C., & Pounds, K. A. 1993, ARA&A, 31, 717

- Mushotzky, R. F., Fabian, A. C., Iwasawa, K., Matsuoka, M., Nandra, K., Tanaka, Y. 1995, MNRAS 272, L9
- Nagao, T., Murayama, T., & Taniguchi, Y. 1999a, ApJ, submitted
- Nagao, T., Murayama, T., Taniguchi, Y., & Yoshida, M. 1999b, AJ, submitted
- Nandra, K., George, I. M., Mushotzky, R. F., Turner, T. J., & Yaqoob, T. 1997, ApJ, 477, 602
- Nandra, K., & Pounds, K. A. 1994, MNRAS, 268, 405
- Netzer, H., & Laor, A. 1993, ApJ, 404, L51
- Nishiura, S., Murayama, T., & Taniguchi, Y. 1998, PASJ, 50, 31
- Nishiura, S., & Taniguchi, Y. 1998, ApJ, 499, 134
- Norman, C. A., & Miley, G. K. 1984, A&A, 141, 85
- Osterbrock, D. E. 1989, Astrophysics of Gaseous Nebulae and Active Galactic Nuclei (San Francisco, Freeman)
- Osterbrock, D. E., & Pogge, R. W. 1985, ApJ, 297, 166 (OP85)
- Osterbrock, D. E., & Shaw, R. 1988, ApJ, 328, 89
- Padovani, P. 1989, 209, 27
- Padovani, P., Burg, R., & Edelson, R. A. 1990, ApJ, 353, 438
- Padovani, P., & Rafanelli, P. 1988, A&A, 205, 53
- Persson, S. E. 1988, ApJ, 330, 751
- Peterson, B. M. 1993, PASP, 105, 247
- Peterson, B. M. 1997, An Introduction to Active Galactic Nuclei, (Cambridge University Press, Cambridge)
- Phillips, M. M. 1978, ApJs, 38, 187
- Pier, E., & Voit, M. 1995, ApJ, 450, 628
- Pogge, R. W. 1989, ApJ, 345, 730
- Pounds, K., Done, C., & Osborne, J. 1995, MNRAS, 277, L5
- Pringle, J. MNRAS, 292, 136
- Puchnarewicz, E. M., Branduardi-Raymont, G., Mason, K. O., & Sekiguchi, K. 1995a, MNRAS, 276, 1281
- Puchnarewicz, E. M., Mason, K. O., Córdova, F. A., Kartje, J., Branduardi-Raymont, G., Mittaz, J. P. D., Murdin, P. G., & Allington-Smith, J. 1992, MNRAS, 256, 589
- Puchnarewicz, E. M., Mason, K. O., Romero-Colmenero, E., Carrera, F. J., Hasonger, G., McMahon, R., Mittaz, J. P. D., Page, M. J., & Carballo, R. 1996, MNRAS, 281, 1243
- Puchnarewicz, E. M., Mason, K. O., Siemiginowska, A., & Pounds, K. A. 1995b, MNRAS, 276, 20
- Peterson, B. M. 1993, PASP, 105, 247
- Rees, M. J. 1984, ARA & A, 22, 471
- Reynolds, C. S. 1997, MNRAS 286, 513
- Robinson, A. 1995, MNRAS, 272, 647
- Rodríguez-Pascual, P., Mas-Hesse, J. M., & Santos-Lleó, M. 1997, A&A, 327, 72
- Ross, R. R., & Fabian, A. C. 1993, MNRAS, 261, 74
- Ross, R. R., Fabian, A. C., & Mineshige, S. 1992, MNRAS, 258, 189
- Salzer, J. 1989, ApJ, 347, 152
- Schmitt, H. R., & Kinney, A. L. 1996, ApJ, 463, 498
- Steiner, J. E. 1981, ApJ, 250, 469
- Stephens, S. A. 1989, AJ, 97, 10
- Sulentic, J. W., & Marziani, P. 1999, ApJ, 518, L9
- Sulentic, J. W., Marziani, P., Dultzin-Hacyan, D., Calvani, M., & Moles, M. 1995, ApJ, 445, L85
- Tanaka, Y. 1990, The 23rd ESLAB Symp. on X-ray Astronomy, eds. J. Hunt, and B. Battruck (ESA SP-296), 3
- Tanaka, Y., et al. 1995, Nature, 375, 659
- Taniguchi, Y., & Anabuki, N. 1999, ApJ, 521, L103
- Taniguchi, Y., Dultzin-Hacyan, D., & Murayama, T. 1999, in preparation
- Taniguchi, Y., & Murayama, T. 1998, ApJ, 501, L25
- Taniguchi, Y., Sato, Y., Kawara, K., Murayama, T., & Mouri, H. 1997, A&A, 318, L1
- Tran 1995, ApJ, 440, 597
- Ulvestad, J. S., Antonucci, R. J., & Goodrich, R. W. 1995, AJ, 109, 81
- Ulvestad, J. S., & Wilson, A. S. 1989, ApJ, 343, 659
- Urry, C. M., & Padovani, P. 1995, PASP, 107, 803
- van Groningen, E., & de Bruyn, A. G. 1989, A & A, 211, 293
- Vaughan, S., Reeves, J., Warwick, R., & Edelson, R. 1999, MNRAS, in press (astro-ph/9905323)
- Walter, R., & Fink, N. H. 1993, A&A, 274, 105
- Wanders, I., et al. 1995, ApJ, 453, L87
- Wandel, A., & Boller, T. 1998, A&A, 331, 884
- Wandel, A., Peterson, B. M., & Malkan, M. A. 1999, ApJ, in press (astro-ph/9905224)
- Wandel, A., & Yahil, A. 1985, ApJ, 295, L1
- Wang, T., Brinkmann, W., & Bergeron, J. 1996, A&A, 309, 81
- White, N., Fabian, A. C., & Mushotzky, R. F. 1984, A&A, 133, L9
- Wilkes, B. J., Elvis, M., & McHardy, I. 1987, ApJ, 321, L23
- Wilson, A. S., & Raymond, J. C. 1999, ApJ, 513, L115
- Wilson, A. S., & Tsvetanov, Z. I. 1994, AJ, 107, 1227
- Wilson, A. S., & Ulvestad, J. S. 1983, ApJ, 275, 8
- Wilson, A. S., Ward, M. J., & Haniff, C. A. 1988, ApJ, 334, 121
- Wolf, S., & Henning, Th. 1999, A&A, 341, 675
- Xu, D. W., Wei, J. Y., & Hu, J. Y. 1999, ApJ, 517, 622
- Zheng, W., & O'Brien, P. T. 1990, ApJ, 353, 433